



Universidad Autónoma  
de Madrid

**Biblos-e Archivo**  
Repositorio Institucional UAM

**Repositorio Institucional de la Universidad Autónoma de Madrid**

<https://repositorio.uam.es>

Esta es la **versión de autor** del artículo publicado en:  
This is an **author produced version** of a paper published in:

Chemical Society Reviews 48.10 (2019): 2738-2766

**DOI:** <https://doi.org/10.1039/C9CS00059C>

**Copyright:** © 2019 The Royal Society of Chemistry

El acceso a la versión del editor puede requerir la suscripción del recurso  
Access to the published version may require subscription

# Phthalocyanines and Porphyrinoid Analogues as Hole- and Electron- Transporting Materials for Perovskite Solar Cells

Maxence Urbani,<sup>a,c</sup> Gema de la Torre,<sup>a,d</sup> Mohammad Khaja Nazeeruddin<sup>\*,b</sup> and Tomás Torres<sup>a,c,d,\*</sup>

Received 00th January 20xx,  
Accepted 00th January 20xx

DOI: 10.1039/x0xx00000x

[www.rsc.org/](http://www.rsc.org/)

Organic-inorganic lead halide perovskite absorbers in combination with electron and hole transporting selective contacts result in power conversion efficiencies of over 23% under AM 1.5 sun conditions. The advantage of perovskite solar cells is their simple fabrication through solution-processing methods either in n-i-p or p-i-n configurations. Using TiO<sub>2</sub> or SnO<sub>2</sub> as an electron transporting layer, compositionally engineered perovskite as absorber layer, and Spiro-OMeTAD as HTM, several groups have reported over 20% of efficiency. Though perovskite solar cells reached comparable efficiency to that of crystalline silicon ones, their stability remains a bottleneck for commercialization partly due to the use of doped Spiro-OMeTAD. Several organic and inorganic hole transporting materials have been explored to increase the stability and power conversion efficiency of perovskite solar cells. In this review, we discuss stable macrocyclic based on phthalocyanines and porphyrins as hole- and electron transporting materials for perovskite solar cells. The  $\pi$ - $\pi$  stacking orientation of these macrocycles on the perovskite surface is important in facilitating a vertical charge transport, resulting in high power conversion efficiency.

## 1. Introduction

Perovskite solar cells (PSC) are a new paradigm in renewable energy because their unparalleled efficiency has increased from 3.8% to 23.7% in less than 10 years.<sup>1,2</sup> The high efficiency of perovskite solar cells is due to their excellent optoelectronic properties, which were optimized by various cations and anions with different ratios.<sup>3</sup> Another advantage of perovskite solar cells is their simple fabrication through solution-processing methods, either in n-i-p or p-i-n configurations.<sup>4,5</sup> The n-i-p configuration consists of a compact TiO<sub>2</sub>, and mesoporous TiO<sub>2</sub> layers to transport electrons from the perovskite absorber to the contact.<sup>4</sup> The perovskite absorbing layer consisting of methyl ammonium lead (II) iodide (MAPbI<sub>3</sub>) is intrinsically unstable at elevated temperature due to methylammonium cation release.<sup>6,7</sup> Therefore, compositionally engineered cations and anions are deposited using either one-step or two-step methods.<sup>4</sup> The compositionally engineered [FA<sub>0.8</sub>MA<sub>0.15</sub>CS<sub>0.05</sub>PbI<sub>(3-x)</sub>Br<sub>x</sub>] three-dimensional (3D) perovskite shows excellent absorption properties, low exciton binding energy and high charge carrier mobilities (with MA = methylammonium, and FA = formamidinium).<sup>8</sup> Using mixed cations, anions and solvent engineering method, power conversion efficiencies (PCE) of 3D perovskite solar cells have

reached over 23%.<sup>2</sup> The performance of perovskite solar cells depends on the formation of over-layer thickness that is controlled by inverse solubility, and solvent engineering technique.<sup>9,10</sup> Finally, a hole transporting layer (HTL) followed by a gold contact is deposited to complete the cell. The perovskite solar cells using 2,2',7,7'-tetrakis(*N,N'*-di-*p*-methoxyphenylamine)-9,9'-spirobifluorene (Spiro-OMeTAD) as hole-transporting material (HTM) are less stable compared to poly[bis(4-phenyl)(2,5,6-trimethylphenyl) amine (PTAA) polymer based HTM due to doping and additives.<sup>11</sup>

The performance of 3D perovskite solar cells decreases under heat and light soaking conditions due to ion migration and segregation.<sup>12</sup> The other detrimental drawback of 3D perovskites is their poor moisture stability, due to the ionic nature of the materials and their low formation energies, which make them vulnerable for water-induced hydrolysis.<sup>13</sup> Though there are several approaches to stabilize the 3D perovskite, the most common one is cation tuning.<sup>14</sup> The bigger cations beyond the Goldsmith tolerance limit produce low dimensional perovskites, which are very stable but have larger bandgaps and higher exciton binding energies than 3D perovskites.<sup>15</sup> Nevertheless, the exceptional stability under heat and light soaking conditions of low-dimensional perovskites makes them an essential family of materials, and the prospects to integrate these exciting novel materials to protect the highly efficient 3D perovskites and, therefore, to increase their stability, are enormous. Using hot casting techniques, a two-dimensional (2D) perovskite incorporated in the bulk of 3D perovskite yielded 12.5% PCE, and increased stability over 2250 hours.<sup>16</sup> Also, the composition of perovskite absorber has been optimized using 2D perovskite, and stable performance over 12000 h without HTM is reported.<sup>17</sup> In these cells a triple layer

<sup>a</sup> Departamento de Química Orgánica, Universidad Autónoma de Madrid, Cantoblanco, 28049 Madrid, Spain. E-mail: [tomas.torres@uam.es](mailto:tomas.torres@uam.es)

<sup>b</sup> Group for Molecular Engineering of Functional Materials, Institute of Chemical Sciences and Engineering, EPFL, Valais Wallis, Rue de l'Industrie 17, 1950 Sion, Switzerland. E-mail: [mdkhaja.nazeeruddin@epfl.ch](mailto:mdkhaja.nazeeruddin@epfl.ch)

<sup>c</sup> IMDEA-Nanociencia, Campus de Cantoblanco, 28049 Madrid, Spain.

<sup>d</sup> Institute for Advanced Research in Chemical Sciences (IAChem) Universidad Autónoma de Madrid, 28049 Madrid, Spain.

architecture having  $\text{ZrO}_2$  as an insulating layer and conducting carbon is used both as HTL and contact. The triple layer carbon-based PSC data demonstrate that the organic HTM in these cells is still the bottleneck for commercial applications.

Also, the electron transporting layer (ETL)  $\text{TiO}_2$  influences the stability of PSCs due to its unfavourable properties including singlet oxygen generation caused by UV light, high temperature sintering process and UV instability.<sup>18</sup> Among the various device architectures, the n-i-p planar structure has attracted a lot of attention because of the low temperatures needed for the processing of the ETLs. Recently, various ETLs have been explored, and  $\text{SnO}_2$  emerged as an ideal material for perovskite solar cells, because of its higher electron mobility, low-temperature processing, and UV-stability.<sup>19</sup> Using passivated  $\text{SnO}_2$  as ETL, compositionally engineered perovskite as absorbing layer, and Spiro-OMeTAD as HTM, several groups have reported PCEs over 20%.<sup>20</sup> A bilayer configuration involving a compact layer of  $\text{TiO}_2$  and low temperature deposited  $\text{SnO}_2$  displays better energy level alignment with the perovskite, resulting in a PCE over 22% with an open circuit voltage ( $V_{\text{oc}}$ ) close to 1.14 V, a short circuit current ( $J_{\text{sc}}$ ) of 24.78  $\text{mA}/\text{cm}^2$ , a fill factor (FF) of 0.78, and a negligible J-V hysteresis in the device.

To date, Spiro-OMeTAD and PTAA are the hole transporting materials of choice routinely employed in PSC under normal configuration (n-i-p) in order to maintain the highest efficiency. However, their challenging synthesis and prohibitively high price hinder the progress towards low-cost PSC manufacturing, and may contribute to more than 30% of the overall module price. The reason resides in the complicated multi-step synthetic procedure of Spiro-OMeTAD, together with the high-purity, sublimation-grade that is required to obtain high-performance devices. In inverted-type PSC (p-i-n), the conventional HTL is usually the conductive polymer PEDOT:PSS but it suffers from several drawbacks.<sup>21</sup> The two first ones concern stability matters owing to its hygroscopic and acidic nature, which may accelerate degradation of the perovskite layer and corrode the FTO glass substrate, respectively. The third one is its limited capability for blocking the backflow of electrons from the perovskite layer, thus restricting the efficiency of inverted-PSCs.

Also, the use of dopants to increase mobility is problematic, and can induce instability of the device.<sup>22</sup> Furthermore, the hygroscopic nature of the additive salts such as bis(trifluoromethane)sulfonimide lithium salt (LiTFSI) makes the HTL highly hydrophilic, showing a tendency towards chemical degradation, negatively influencing the stability of the entire device. Moreover, the additive *tert*-butylpyridine (TBP) has been revealed to interact with perovskite and may dissolve it, inducing corrosion phenomenon, and even may cause a chemical reaction with the HTM.

Another interesting class of HTM is based on macrocycle molecules such as phthalocyanines (Pcs) and porphyrins (Pors), which are thermally and photochemically stable. The optical and electronic properties of these macrocycles can be easily adjusted by modifying the peripheral and non-peripheral substituents and the metal center. As a consequence of their

preeminent role in nature, porphyrins and their analogues are customary chromophores to be employed as components of photovoltaic and artificial photosynthetic devices. For instance, ZnPors<sup>23,24</sup> and ZnPcs<sup>25</sup> have been largely used as photosensitizers for DSSCs, and particularly, push-pull ZnPors decorated with opposite donor and acceptor/anchoring groups have shown record high conversion efficiencies of up to 13%.<sup>26</sup> In the past few years, several groups have also investigated and proved that Pcs and Pors can be successfully incorporated as HTM in perovskite solar cells, as will be highlighted in this review.

## 2. Phthalocyanines for perovskite solar cells

Phthalocyanines (Pcs) are blue pigments with strong absorption features in the red/NIR region. In this regard,<sup>27</sup> a key question arises: Would the light-harvesting properties of Pcs negatively affect the efficiency of PSCs? In principle, the HTM layer should be preferably colourless to avoid light absorption losses of the perovskite layer. Although their strong absorption may entail a drawback for PSC applications, the number of advantages such as versatility, robustness (thermal, chemical and solar irradiation) and low-cost of production, to name a few, make up for the absorption issue. Another advantage of Pcs is their strong tendency to aggregate through  $\pi$ - $\pi$  stacking interactions,<sup>28</sup> an inherent property that has been largely exploited for self-organization at the supramolecular level.<sup>29–32</sup> In solid thin film devices technology, the degree of aggregation of Pc molecules is known to affect drastically the crystallinity and morphology of the Pc-films, which are critical toward conductivity of the active layer (and hence overall efficiency). In particular, several  $\alpha$ -<sup>33–38</sup> and  $\beta$ -<sup>39–42</sup> substituted Pcs functionalized with terminal alkyl chains have shown the ability to form highly condensed and ordered phases in liquid crystalline films by spontaneous molecular alignment into columnar stacks, which enhance drastically the charge transport and renders them excellent organic semiconductor materials for application in thin film devices, such as organic field effect transistors (OFET)<sup>43</sup> and solar cells. Ambipolar behaviour and conductivity values as high as  $1.4 \text{ cm}^2 \cdot \text{V}^{-1} \cdot \text{s}^{-1}$  have been obtained with these Pc-films.<sup>33</sup> In this context, it is not surprising that Pcs show a great potential to be incorporated as hole selective layer (so far, almost exclusively as p-type HTL) in the architecture of perovskite solar cells (*meso* or planar), both in normal (n-i-p) or inverted (p-n-i) configurations. Another major purpose of introducing Pcs into these devices is to protect efficiently the perovskite layer from moisture degradation, and thus to improve long-term stability.

The Pc hole-transporting material can be included in different ways, either as a single-layer (neat/pristine, doped or composite) or integrated in a multi-junctions HTL, the latter including bi-, buffer- or hybrid interfacial buffer (infiltrated HTM) layers. Another less known use of Pcs in the field of PSC is that of chemical dopant of other HTMs or the perovskite material itself, which have been reported more recently. The synthetic versatility of these macrocycles, both from the Pc scaffold ( $\alpha$ - and  $\beta$ -positions)<sup>44</sup> and metal centre, offers many

possibilities to engineer new functional Pc-materials for such application:

- Tailoring the Pc macrocycle with hydrophobic groups (*e.g.* alkyl chains) aims to enhance the overall stability of the PSCs by protecting the perovskite layer from moisture.
- Introduction of solubilizing groups facilitates solution-processed fabrication of the Pc-selective layer (usually by spin-coating) thus reducing the cost of fabrication in comparison, for instance, with thermal vacuum deposition methods (*vide infra*).
- Introduction of substituents of different size (small or bulky) may change the degree of aggregation of the Pc, and thus help to control the morphology and crystallinity of the Pc-films.
- Introduction of more elaborated groups (*e.g.* heteroaryl or conjugated systems), modulates their optoelectronic and electrochemical properties (in addition to aggregation behaviour).
- A Pc can be metal-free ( $H_2Pc$  or free-base) or metallated (MPc) with many different kinds of metal ions that can be accommodated in the central cavity of the macrocycle (Zn, Cu, Mg, Fe, Ni, Ru, Pd, Co, Pb, Ti, V, Ge), which strongly affect their intrinsic properties (topological, optical, electrochemical and energetics), as well as their aggregation behaviour.

Regarding the molecular design, a large variety of Pcs has been explored for PSC applications, which can be divided in four main classes of compounds:

- Unsubstituted Pcs (Fig. 1 and Table 1)
- Symmetrically and peripherally ( $\beta$ ) substituted Pcs, comprising  $\beta$ -tetrakis (Fig. 2 and Table 2) and  $\beta$ -octakis (Fig. 3 and Table 3) patterns.
- Symmetrically and non-peripherally ( $\alpha$ ) substituted Pcs, comprising  $\alpha$ -tetrakis (Fig. 4 and Table 4) and  $\alpha$ -octakis (Fig. 5 and Table 5) patterns.
- Unsymmetrically substituted Pcs (AAAB-type; Fig. 6 and Table 6)

Unsubstituted metal-Pcs (**CuPc**, **NiPc**, **PbPc**, **ZnPc**, **TiOPc** and **V(O)Pc**; Fig. 1 and Table 1) are distinguished by i) simplicity of synthesis and low cost of production (most of them are commercially available), ii) insolubility or poor solubility in most common solvents, iii) high degree of aggregation, and iv) they

can be sublimated. These above-mentioned properties have pros and cons for practical utilisation in PSCs.

In solution-processed techniques, this implies to use these Pcs at very low concentrations, therefore making them suitable only as dopant, but turning out to be unrealistic for the fabrication of a Pc-(HTM) single layer; for the latter case, thermal vacuum deposition (VD) is the method of choice since most of these Pcs can be sublimated. However, VD is a more complex and highly energy-consuming (hence expensive) process of fabrication, thus counter-balancing the low-cost facet of the Pc material. In turn, it presents the advantages to guarantee high purity of the films and a precise control of the parameters of fabrication (rate of deposition, layer thickness, etc.), which hence confers high reproducibility to this method. Moreover, since no organic nor toxic solvent is involved at this stage, part of the cost and environmental impact are reduced. The most important benefit is that they do not require dopants due to aggregation, which is advantageous in term of cost and stability.

Further changes in the molecular design came with the introduction of methyl or ethyl chains in  $\beta$ -tetrakis-substituted Pcs (**Cu-1a** and **Cu-2**; Fig. 2 and Table 2) or  $\beta$ -octakis analogues (**2H-1b**, **Zn-1b**, **Cu-1b** and **Pd-1b**; Fig. 3 and Table 3). These short alkyl chains still allow vacuum deposition method for the fabrication of the HTM layer, and induce important changes in the properties of the Pc-films (morphological in particular).  $\beta$ -tetrakis substituted Pcs with longer alkyl chains (*n*-propyl, *n*-butyl, *tert*-butyl) no longer allow VD but solution-processed techniques instead. A myriad of other functional groups have been reported for  $\beta$ -tetrakis substituted Pcs (sulfonyl, ammonium, aryl, heteroaryl; Fig. 2 and Table 2) as well as their  $\beta$ -octakis fully substituted versions (Fig. 3 and Table 3). In a lesser extent, non-peripheral substitution pattern has also been envisaged for Pc-based HTMs, and as well,  $\alpha$ -octakis (Fig. 4 and Table 4) and  $\alpha$ -tetrakis (Fig. 5 and Table 5) substituted versions have been explored. Finally, a fourth class of Pc-HTMs having a non-symmetrical substitution pattern (AAAB-type; Fig. 6 and Table 6), has also been tested more recently in PSCs, though very few examples were reported.

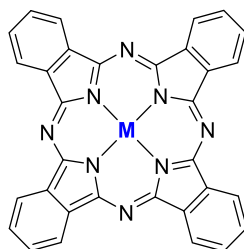


Fig. 1 General structure of unsubstituted phthalocyanines (M = metal).

Table 1. Role and work function ( $W_F$ ) of unsubstituted Pcs (see Fig. 1) employed in PSC, and photovoltaic performances of the champion devices under different configuration ( $m$  = mesoporous,  $P$  = planar and  $IP$  = inverted planar).<sup>a</sup>

Pc	M =	Role	$W_F^b$ (eV)	Perovskite composition	Architecture	Type	$J_{sc}$ (mA/cm <sup>2</sup> )	$V_{oc}$ (V)	F.F. (%)	PCE (%)	Ref
CuPc	Cu	HTM	(-5.2) <sup>c</sup>	MAPbI <sub>3-x</sub> Cl <sub>x</sub>	FTO/cTiO <sub>2</sub> /mTiO <sub>2</sub> /perov./CuPc/Au	$m$	16.3	0.75	40	5.0	44
		HTM	(-5.2) <sup>c</sup>	MAPbI <sub>3</sub>	FTO/cTiO <sub>2</sub> /mTiO <sub>2</sub> /perov./CuPc/Au	$m$	20.14	1.04	71	14.89	45
		HTM	(n/a)	MAPbI <sub>3</sub>	FTO/cTiO <sub>2</sub> /mTiO <sub>2</sub> /perov./CuPc/carbon	$m$	22.65	1.027	71.4	16.61	46
		HTM	(-5.2) <sup>c</sup>	MAPbI <sub>3</sub>	FTO/cTiO <sub>2</sub> /mTiO <sub>2</sub> /perov./CuPc/carbon	$m$	20.8	1.05	74	16.1	47
		HTM	(-5.2) <sup>c</sup>	MAPbI <sub>3</sub>	FTO/C <sub>60</sub> /perov./Pc/Au	$P$	19.13	1.04	77.47	15.42	48
		HTM	(-5.2) <sup>c</sup>	MAPbI <sub>3</sub>	FTO/SnO <sub>2</sub> /perov./CuPc/Au	$P$	23.17	0.939	44.1	9.6	49
		HTM	(-5.2) <sup>c</sup>	MAPbI <sub>3</sub>	FTO/SnO <sub>2</sub> /PCBM/perov./CuPc/Au	$P$	19.37	1.045	62	12.55	50
		HTM	(-5.2) <sup>c</sup>	CS <sub>0.05</sub> (MA <sub>0.17</sub> FA <sub>0.83</sub> ) <sub>0.95</sub> Pb(I <sub>0.83</sub> Br <sub>0.17</sub> ) <sub>3</sub>	FTO/TiO <sub>2</sub> /SnO <sub>2</sub> /perov./CuPc/carbon	$P$	23.28	0.98	67	15.39	51
		HTM	(-5.2) <sup>c</sup>	MAPbI <sub>3</sub>	ITO/CuPc/perov./PCBM/BCP/Ag	$IP$	18.9	0.96	80	14.5	52
		HTM	(-5.2) <sup>c</sup>	CS <sub>0.05</sub> FA <sub>0.81</sub> MA <sub>0.14</sub> PbI <sub>2.55</sub> Br <sub>0.45</sub>	ITO/CuPc/perov./PCBM/BCP/Ag	$IP$	19.4	1.03	77	15.4	52
		HTM (buffered)	-5.28 <sup>UPS/SKP</sup>	MAPbI <sub>3</sub>	ITO/VOx/CuPc/perov./C <sub>60</sub> /BCP/Ag	$IP$	22.15	1.015	74.8	16.85	53
ZnPc	Zn	Dopant (of perov.)	(n/a)	MAPbI <sub>3</sub> +CuPc(0.05 wt%)	FTO/cTiO <sub>2</sub> /mTiO <sub>2</sub> /(perov.+CuPc)/Spiro/Au	$m$	15.30	0.88	61.7	8.4	54
		HTM	(-5.2) <sup>c</sup>	MAPbI <sub>3</sub>	FTO/cTiO <sub>2</sub> /mTiO <sub>2</sub> /perov./ZnPc/Au	$m$	10.4	0.774	43.5	3.50	55
		Bi-HTM Buffer	(n/a)	MAPbI <sub>3</sub>	FTO/Nb-TiO <sub>x</sub> /Perov/ZnPc/Spiro/Au	$P$	22.5	1.07	0.70	16.8	56
		Bi-HTM Buffer	(n/a)	MAPbI <sub>3-x</sub> Cl <sub>x</sub>	FTO/cTiO <sub>2</sub> /perov./ZnPc/Spiro/Au	$P$	21.2	1.04	75.3	16.7	57
		Bi-HTM Buffer	(n/a)	MAPbI <sub>3-x</sub> Cl <sub>x</sub>	FTO/cTiO <sub>2</sub> /SAED/perov./ZnPc/Spiro/Au	$P$	21.7	1.09	75.8	17.8	57
		HTM	-5.28 <sup>UPS, 58</sup>	MAPbI <sub>3</sub>	ITO/ZnPc/perov./C <sub>60</sub> /BCP/Al	$IP$	17.3	0.96	70	11.6	59
PbPc	Pb	HTM	(-5.0) <sup>c</sup>	MAPbI <sub>3</sub>	FTO/cTiO <sub>2</sub> /mTiO <sub>2</sub> /perov./PbPc/Au	$m$	13.4	0.816	36.3	3.97	55
		HTM	(-5.2) <sup>c</sup>	MAPbI <sub>3</sub>	ITO/CuI/PbPc/perov./C <sub>60</sub> /Bphen/Ag	$IP$	20.49	0.80	66	10.79	60
TiOPc	Ti(O)	HTM	(-5.4) <sup>c</sup>	MAPbI <sub>3</sub>	FTO/cTiO <sub>2</sub> /mTiO <sub>2</sub> /perov./TiOPc/Au	$m$	12.86	0.737	54	5.05	61
VOPc	V(O)	HTM	(n/a)	MAPbI <sub>3</sub>	FTO/cTiO <sub>2</sub> /mTiO <sub>2</sub> /perov./VOPc/Au	$m$	11.26	0.76	28	2.44	62
NiPc	Ni	HTM	(-5.0) <sup>c</sup>	MAPbI <sub>3</sub>	FTO/cTiO <sub>2</sub> /perov./NiPc/Au	$P$	17.64	0.94	73	12.1	63
		Dopant (of perov.)	(n/a)	CS <sub>0.05</sub> (MA <sub>0.17</sub> FA <sub>0.83</sub> ) <sub>0.95</sub> Pb(I <sub>0.83</sub> Br <sub>0.17</sub> ) <sub>3</sub> +NiPc	FTO/TiO <sub>2</sub> /(perov.+NiPc)/Spiro/Au	$P$	23.39	1.10	74.78	19.18	64

<sup>a</sup>Abbreviations: **BCP** = bathocuproine; **Bi-HTM** = HTM within a bilayer configuration; **Bphen** = bathophenanthroline (4,7-diphenyl-1,10-phenanthroline); **cTiO<sub>2</sub>** = compact TiO<sub>2</sub> (blocking layer); **FA** = formylamidinium; **FTO** = fluorine doped tin oxide; **HTM** = hole transporting material; **ITO** = indium doped tin oxide; **MA** = methylammonium; **mTiO<sub>2</sub>** = mesoporous TiO<sub>2</sub>; **Pc** = phthalocyanine; **perov.** = perovskite; **PCMB** = 6,6-phenyl C<sub>61</sub> butyric acid methyl ester; **SAED** = SrAl<sub>2</sub>O<sub>4</sub> doped with Eu<sup>2+</sup> and Dy<sup>3+</sup>; **Spiro** = Spiro-OMeTAD (2,2',7,7'-tetrakis(*N,N*-di-*p*-methoxyphenylamine)-9,9'-spirobifluorene). <sup>b</sup>Work function ( $W_F$ ) of the Pc-based layer (UPS: determined by ultraviolet photoelectron spectroscopy measurements; SKP: determined by surface Kelvin probe measurements). <sup>c</sup>Method of determination not reported in the original article. <sup>d</sup>NiPc (0.5 mg·ml<sup>-1</sup> in chlorobenzene) was introduced *via* a mixed-anti solvent technique prior to completion of the perovskite crystals.

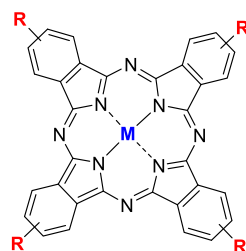
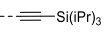
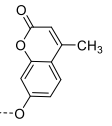
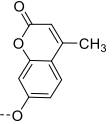
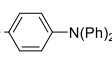
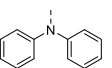
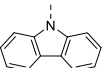
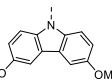
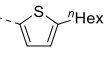
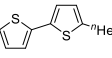


Fig. 2 General structures of  $\beta$ -(tetrakis)substituted phthalocyanines (M = metal).

Table 2. Work function ( $W_F$ ) and role of  $\beta$ -(tetrakis)substituted Pcs (see Fig. 2) employed in PSC, and photovoltaic performances of the champion devices under different configuration ( $m$  = mesoporous, P = planar and IP = inverted planar).<sup>a</sup>

Pc	R =	M =	$W_F^b$ (eV)	Role	Perovskite composition	Architecture	Type	$J_{sc}$ (mA/cm <sup>2</sup> )	$V_{oc}$ (V)	F.F. (%)	PCE (%)	Ref
Cu-1a	CH <sub>3</sub>	Cu	(-5.12) <sup>CV</sup>	HTM	MAPbI <sub>3-x</sub> Cl <sub>x</sub>	FTO/cTiO <sub>2</sub> /mTiO <sub>2</sub> /perov./Pc/Au	<i>m</i>	16.9	0.70	40	5.2	65
			(-5.1) <sup>S</sup>	HTM	MAPbI <sub>3</sub>	FTO/SnO <sub>2</sub> /perov./Pc/Au	P	23.19	0.972	52.9	11.9	49
Cu-2	C <sub>2</sub> H <sub>5</sub>	Cu	(-5.1) <sup>S</sup>	HTM	MAPbI <sub>3</sub>	FTO/SnO <sub>2</sub> /perov./Pc/Au	P	22.59	1.02	50.7	11.7	49
Cu-3	<sup>n</sup> C <sub>3</sub> H <sub>7</sub>	Cu	(-4.92) <sup>PS</sup> (-5.13) <sup>EC</sup>	HTM	MAPbI <sub>3</sub>	FTO/SnO <sub>2</sub> /perov./Pc/Au	P	23.2	1.01	76	17.80	66
Cu-4	<sup>n</sup> C <sub>4</sub> H <sub>9</sub>	Cu	(-5.2) <sup>EC,70</sup>	HTM (+add.)	MAPbI <sub>3-x</sub> Cl <sub>x</sub>	FTO/cTiO <sub>2</sub> /mTiO <sub>2</sub> /perov./Pc/Au	<i>m</i>	17.0	0.89	48	7.3	67
			(-5.2) <sup>EC,70</sup>	(+add. & buff.)	MAPbI <sub>3-x</sub> Cl <sub>x</sub>	FTO/cTiO <sub>2</sub> /mTiO <sub>2</sub> /perov./Al <sub>2</sub> O <sub>3</sub> :Pc/Au	<i>m</i>	19.5	0.99	50	9.7	67
			(-5.2) <sup>EC,70</sup>	HTM (+add. & buff.)	MAPbI <sub>3-x</sub> Cl <sub>x</sub>	FTO/cTiO <sub>2</sub> /mTiO <sub>2</sub> /perov./GO:Pc/Au	<i>m</i>	20.9	1.04	66	14.4	67
			(-5.2) <sup>EC,70</sup>	HTM (buff.)	[MAPbI <sub>3-x</sub> Cl <sub>x</sub> ] wt%]	FTO/cTiO <sub>2</sub> /mTiO <sub>2</sub> /RGO(0.2% wt%)/perov./GO:Pc/Au	<i>m</i>	21.0	1.07	71	15.9	68
			(-5.2) <sup>EC,70</sup>	HTM	MAPbI <sub>3-x</sub> Cl <sub>x</sub>	FTO/cTiO <sub>2</sub> /mTiO <sub>2</sub> /perov./Pc/Au	<i>m</i>	17.3	0.89	56	8.5	69
			( <i>n/a</i> )	Dopant (of HTM; +add.)	MAPbI <sub>3-x</sub> Cl <sub>x</sub>	FTO/cTiO <sub>2</sub> /mTiO <sub>2</sub> /perov./[Spiro-90%+Cu Pc(10%)]/Au	<i>m</i>	24.9	0.97	64	15.4	70
Cu-5	<i>tert</i> -butyl	Cu	( <i>n/a</i> )	HTM	MAPbI <sub>3-x</sub> Cl <sub>x</sub>	FTO/cTiO <sub>2</sub> /mTiO <sub>2</sub> /perov./Pc/Au	<i>m</i>	13.8	0.94	43	5.6	69
			(-5.22) <sup>S</sup>	HTM (+add.)	(FAPbI <sub>3</sub> ) <sub>0.85</sub> (MAPbBr <sub>3</sub> ) <sub>0.15</sub>	FTO/cTiO <sub>2</sub> /mTiO <sub>2</sub> /perov./Pc/Au	<i>m</i>	21.9	1.045	66.35	15.2	71
			(-5.2) <sup>S</sup>	HTM (+add.)	(FAPbI <sub>3</sub> ) <sub>0.85</sub> (MAPbBr <sub>3</sub> ) <sub>0.15</sub>	FTO/cTiO <sub>2</sub> /mTiO <sub>2</sub> /perov./Pc/Au	<i>m</i>	22.6	1.07	77.5	18.8	72
			(-5.20) <sup>UPS</sup>	HTM (+add.)	CS <sub>0.07</sub> Rb <sub>0.03</sub> FA <sub>0.765</sub> MA <sub>0.135</sub> PbI <sub>2.55</sub> Br <sub>0.45</sub>	ITO/cTiO <sub>2</sub> /mTiO <sub>2</sub> /PCBM+PMMA/ perov./Pc/Au	<i>m</i>	23.6	1.147	74.2	20.09	73
			(-5.20) <sup>EC</sup>	HTM	CS <sub>0.05</sub> (FA <sub>0.83</sub> MA <sub>0.17</sub> ) <sub>0.95</sub> Pb(I <sub>0.9</sub> Br <sub>0.1</sub> ) <sub>3</sub>	FTO/RTA-TiO <sub>2</sub> /perov./Pc/Au	P	22.1	1.04	60	13.7	74
			(-5.20) <sup>EC</sup>	HTM (buff.)	CS <sub>0.05</sub> (FA <sub>0.83</sub> MA <sub>0.17</sub> ) <sub>0.95</sub> Pb(I <sub>0.9</sub> Br <sub>0.1</sub> ) <sub>3</sub>	FTO/RTA-TiO <sub>2</sub> /perov./Al <sub>2</sub> O <sub>3</sub> :Pc/Au	P	23.4	1.05	60	14.8	74
			( <i>n/a</i> )	Dopant (of perov.)	(MAPbI <sub>3-x</sub> Cl <sub>x</sub> ) <sub>1-n</sub> (Pc) <sub>n</sub>	FTO/TiO <sub>2</sub> /perov.+Pc/Spiro/Au	P	22.6	1.02	75	17.3	75
			( <i>n/a</i> )	Dopant (of HTM; +add.)	(FAPbI <sub>3</sub> ) <sub>0.85</sub> (MAPbBr <sub>3</sub> ) <sub>0.15</sub>	FTO/cTiO <sub>2</sub> /mTiO <sub>2</sub> /perov./Spiro-Pc (4.8 wt%)/Au	<i>m</i>	22.6 (22.3) <sup>av.</sup>	1.14 (1.11) <sup>av.</sup>	77.6 (74.7) <sup>av.</sup>	20.0 (18.5) <sup>av.</sup>	71
Zn-5	<i>tert</i> -butyl	Zn	(-5.31) <sup>EC</sup>	HTM	MAPbI <sub>3</sub>	FTO/cTiO <sub>2</sub> /mTiO <sub>2</sub> /perov./Pc/Au	<i>m</i>	16.29	0.918	53.3	7.98	76
			(-5.32) <sup>EC</sup>	HTM (+add.)	(FAPbI <sub>3</sub> ) <sub>0.85</sub> (MAPbBr <sub>3</sub> ) <sub>0.15</sub>	FTO/cTiO <sub>2</sub> /mTiO <sub>2</sub> /perov./Pc/Au	<i>m</i>	21.75 20.19 <sup>av.</sup>	1.01 1.03 <sup>av.</sup>	68.7 66.3 <sup>av.</sup>	14.48 13.3 <sup>av.</sup>	77
			( <i>n/a</i> )	HTM (+add.)	FA <sub>0.1</sub> MA <sub>0.9</sub> PbI <sub>3</sub>	FTO/cTiO <sub>2</sub> /mTiO <sub>2</sub> /perov./Pc/Au	<i>m</i>	20.23	1.05	66	14.0	78
Ge-5	<i>tert</i> -butyl	GeL <sub>2</sub>	( <i>n/a</i> )	Dopant (of HTM)	MAPbI <sub>3</sub>	FTO/cTiO <sub>2</sub> /mTiO <sub>2</sub> /perov./Spiro+Pc (12.5 wt%)/Au	<i>m</i>	15.81	0.74	46	4.47	62

Cu-6		Cu	$-5.42^{\text{EC}}$	HTM	(FAPbI <sub>3</sub> ) <sub>0.85</sub> (MAPbBr <sub>3</sub> ) <sub>0.15</sub>	FTO/cTiO <sub>2</sub> /mTiO <sub>2</sub> /perov./Pc/carbon	m	1.01	21.4	65	14.0	79
Ni-7		Ni	$-5.25^{\text{th}}$	HTM	(FAPbI <sub>3</sub> ) <sub>0.85</sub> (MAPbBr <sub>3</sub> ) <sub>0.15</sub>	FTO/cTiO <sub>2</sub> /mTiO <sub>2</sub> /perov./Pc/Au	m	19.50	1.061	49.4	10.23	80
Fe-7		Fe	$-5.24^{\text{th}}$	HTM	(FAPbI <sub>3</sub> ) <sub>0.85</sub> (MAPbBr <sub>3</sub> ) <sub>0.15</sub>	FTO/cTiO <sub>2</sub> /mTiO <sub>2</sub> /perov./Pc/Au	m	18.59	1.051	48.0	9.40	80
Zn-8		Zn	$-5.2^{\text{EC}}$	HTM	MAPbI <sub>3-x</sub> Cl <sub>x</sub>	FTO/cTiO <sub>2</sub> /mTiO <sub>2</sub> /perov./Pc/Au	m	22.1	0.67	40	5.6	81
			$(n/a)$	HTM (+add.)	MAPbI <sub>3-x</sub> Cl <sub>x</sub>	FTO/cTiO <sub>2</sub> /mTiO <sub>2</sub> /perov./Pc/Au	m	16	(n/a)	63	9.0	82
			$(n/a)$	HTM (+add. & buff.)	MAPbI <sub>3-x</sub> Cl <sub>x</sub>	FTO/cTiO <sub>2</sub> /mTiO <sub>2</sub> /perov./Al <sub>2</sub> O <sub>3</sub> :Pc/Au	m	20	(n/a)	72	13.65	82
Zn-9		Zn	$-4.96^{\text{EC}}$	HTM (+add.)	MAPbI <sub>3</sub>	FTO/cTiO <sub>2</sub> /mTiO <sub>2</sub> /perov./Pc/Au	m	16.666	1.014	68.1	11.75	83
Zn-10		Zn	$-5.39^{\text{EC}}$	HTM (+add.)	MAPbI <sub>3</sub>	FTO/cTiO <sub>2</sub> /mTiO <sub>2</sub> /perov./Pc/Au	m	10.693	1.001	59.8	6.65	83
Zn-11		Zn	$-5.18^{\text{EC}}$	HTM (+add.)	MAPbI <sub>3</sub>	FTO/cTiO <sub>2</sub> /mTiO <sub>2</sub> /perov./Pc/Au	m	17.430	1.034	61.0	11.44	83
Zn-12		Zn	$-5.19^{\text{EC}}$	HTM (+add.)	MAPbI <sub>3</sub>	FTO/cTiO <sub>2</sub> /mTiO <sub>2</sub> /perov./Pc/Au	m	8.13	0.796	65.7	4.21	84
			$-5.19^{\text{EC}}$	HTM (+add. & buff.)	MAPbI <sub>3</sub>	FTO/cTiO <sub>2</sub> /mTiO <sub>2</sub> /perov./mAl <sub>2</sub> O <sub>3</sub> :Pc/Au	m	17.2	0.988	74	12.8	84
			$-5.19^{\text{EC}}$	HTM (+add.)	(FAPbI <sub>3</sub> ) <sub>0.85</sub> (MAPbBr <sub>3</sub> ) <sub>0.15</sub>	FTO/cTiO <sub>2</sub> /mTiO <sub>2</sub> /perov./Pc/Au	m	21.05 (20.28) <sup>m</sup>	1.06 (1.05) <sup>m</sup>	78.5 (80.3) <sup>m</sup>	17.5 (17.1) <sup>m</sup>	77
Zn-13		Zn	$-5.15^{\text{EC}}$	HTM (+add.)	(FAPbI <sub>3</sub> ) <sub>0.85</sub> (MAPbBr <sub>3</sub> ) <sub>0.15</sub>	FTO/cTiO <sub>2</sub> /mTiO <sub>2</sub> /perov./Pc/Au	m	19.20 (20.16) <sup>m</sup>	1.11 (1.10) <sup>m</sup>	73.2 (69.4) <sup>m</sup>	15.51 (15.5) <sup>m</sup>	77
Cu-14	SO <sub>3</sub> <sup>-</sup> Na <sup>+</sup>	Cu	$-5.0^{\text{UPS}}$ (undoped)	HTM	MAPbI <sub>3-x</sub> Cl <sub>x</sub>	ITO/Pc/perov./PCBM/Bphen/Ag	IP	18.31	0.78	61	8.71	85
			$-5.1^{\text{UPS}}$	HTM (doped)	MAPbI <sub>3-x</sub> Cl <sub>x</sub>	ITO/[Pc+MoO <sub>3</sub> (15 wt%)]/perov./PCBM/Bphen/Ag	IP	18.80	0.82	66	10.46	85
			$-5.3^{\text{UPS}}$	HTM (doped)	MAPbI <sub>3-x</sub> Cl <sub>x</sub>	ITO/[Pc+F4-TCNQ(2.5 wt%)]/perov./PCBM/Bphen/Ag	IP	21.71	0.96	77	16.14	85
			$-5.0^{\text{UPS}}$ (undoped)	Bi-HTM	MAPbI <sub>3</sub>	FTO/TiO <sub>2</sub> /perov./Spiro/Pc/MoO <sub>3</sub> /Ag	P	22.72	1.04	70	16.69	85
			$-5.1^{\text{UPS}}$	Bi-HTM (doped)	MAPbI <sub>3</sub>	FTO/TiO <sub>2</sub> /perov./Spiro/[Pc+MoO <sub>3</sub> (15 wt%)]/MoO <sub>3</sub> /Ag	P	22.34	1.06	72	17.35	85
			$-5.3^{\text{UPS}}$	Bi-HTM (doped)	MAPbI <sub>3</sub>	FTO/TiO <sub>2</sub> /perov./Spiro/[Pc+F4-TCNQ(2.5 wt%)]/MoO <sub>3</sub> /Ag	P	24.32	1.12	74	20.16	85
			$-4.9^{\text{UPS}}$	HTM	MAPbI <sub>3-x</sub> Cl <sub>x</sub>	ITO/Pc/perov./PCBM/Bphen/Ag	IP	17.17	0.77	51	6.28	86
			$-4.9^{\text{UPS}}$	Bi-HTM	MAPbI <sub>3-x</sub> Cl <sub>x</sub>	ITO/(PEDOT:PSS)/Pc/perov./PCBM/Bphen/Ag	IP	19.76	0.91	60	10.78	86
			$-4.9^{\text{UPS}}$	Bi-HTM	MAPbI <sub>3-x</sub> Cl <sub>x</sub>	ITO/Pc/(PEDOT:PSS)/perov./PCBM/Bphen/Ag	IP	21.33	0.95	65	13.17	86



Ni-14	SO <sub>3</sub> <sup>-</sup> Na <sup>+</sup>	Ni	-5.1 <sup>UPS</sup>	Composite HTM	MAPbI <sub>3-x</sub> Cl <sub>x</sub>	ITO/[(PEDOT:PSS)+Pc(50 wt%)]/perov./PCBM/BPhen/Ag	IP	22.23	1.01	77	17.29	86
			-5.11 <sup>UPS</sup>	HTM	MAPbI <sub>3</sub>	ITO/Pc/perov./PCBM/C <sub>60</sub> /BCP/Ag	IP	19.60	0.93	51	9.29	87
			-5.11 <sup>UPS</sup>	Bi-HTM	MAPbI <sub>3</sub>	ITO/(PEDOT:PSS)/Pc/perov./PCBM/C <sub>60</sub> /BCP/Ag	IP	20.21	1.03	65	13.53	87
			-5.11 <sup>UPS</sup>	Bi-HTM	MAPbI <sub>3</sub>	ITO/Pc/(PEDOT:PSS)/perov./PCBM/C <sub>60</sub> /BCP/Ag	IP	21.63	1.04	69	15.52	87
			-5.14 <sup>UPS</sup>	Dopant (of HTM)	MAPbI <sub>3</sub>	ITO/[(PEDOT:PSS)+Pc(10% wt)]/perov./PCBM/C <sub>60</sub> /BCP/Ag	IP	23.01	1.08	77	18.90	87
Zn-15	NH <sub>3</sub> <sup>+</sup>	Zn	(n/a)	Dopant (of perov.)	3D-[MAPbI <sub>3</sub> ]/2D-[(ZnPC) <sub>0.5</sub> MA <sub>n-1</sub> Pb <sub>n(3n+1)</sub> ]	FTO/cTiO <sub>2</sub> /mTiO <sub>2</sub> /perov./Pc/Co <sup>III</sup> /porphyrins/Au	m	23.55	1.11	77.3	20.26	88

<sup>a</sup>Abbreviations: **add.** = additives (usually LiTFSI and 4-*tert*butylpyridine); **BCP** = bathocuproine; **Bi-HTM** = HTM within a bilayer configuration; **BPhen** = bathophenanthroline (4,7-diphenyl-1,10-phenanthroline); **buff.** = buffered; **cTiO<sub>2</sub>** = compact TiO<sub>2</sub> (blocking layer); **F4-TCNQ** = tetrafluorotetracyanoquinodimethane; **FA** = formylamidinium; **FTO** = fluorine doped tin oxide; **GO** = graphene oxide; **HTM** = hole transporting material; **ITO** = Indium doped tin oxide; **MA** = methylammonium; **mTiO<sub>2</sub>** = mesoporous TiO<sub>2</sub>; **Pc** = phthalocyanine; **perov.** = perovskite; **PCBM** = 6,6-phenyl C<sub>61</sub> butyric acid methyl ester; **PMMA** = poly(methyl) methacrylate; **RGO** = reduced Graphene oxide; **RTA-TiO<sub>2</sub>** = rutile TiO<sub>2</sub> array; **Spiro** = Spiro-OMeTAD (2,2',7,7'-tetrakis(*N,N'*-di-*p*-methoxyphenylamine)-9,9'-spirobifluorene). <sup>b</sup>Work function (*W<sub>F</sub>*) of the Pc-containing junction (UPS: determined by ultraviolet photoelectron spectroscopy measurements; IPS: determined by ionization energy measurement system; EC: value estimated from electrochemical measurements in solutions; th.: value estimated from theoretical calculations). <sup>c</sup>Method of determination not reported in the original article. <sup>d</sup>With L = OSiBu<sub>3</sub>.

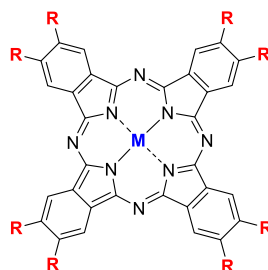


**Fig. 3** General structures of  $\beta$ -(octakis)substituted phthalocyanines (M = metal or 2H).

**Table 3.** Work function (*W<sub>F</sub>*) and role of  $\beta$ -(octakis)substituted Pcs (see Fig. 3) employed in PSC, and photovoltaic performances of the champion devices under different configuration (*m* = mesoporous, *P* = planar).<sup>a</sup>

Pc	R =	M =	<i>W<sub>F</sub></i> <sup>b</sup> (eV)	Role	Perovskite composition	Architecture	Type	<i>J<sub>SC</sub></i> (mA/cm <sup>2</sup> )	<i>V<sub>OC</sub></i> (V)	F.F. (%)	PCE (%)	Ref
2H-1b	CH <sub>3</sub>	2H	(-5.09) <sup>EC</sup>	HTM	MAPbI <sub>3</sub>	FTO/SnO <sub>2</sub> /perov./Pc/Au	P	21.28	1.035	70.8	15.59	89
Zn-1b	CH <sub>3</sub>	Zn	(-5.10) <sup>EC</sup>	HTM	MAPbI <sub>3</sub>	FTO/SnO <sub>2</sub> /perov./Pc/Au	P	21.03	1.005	70.4	14.88	89
Cu-1b	CH <sub>3</sub>	Cu	(-5.1) <sup>EC</sup>	HTM	MAPbI <sub>3</sub>	FTO/SnO <sub>2</sub> /PCBM/perov./Pc/Au	P	1.085	21.32	68	15.73	50
			(-5.11) <sup>EC</sup>	HTM	MAPbI <sub>3</sub>	FTO/SnO <sub>2</sub> /PCBM/perov./Pc/Au	P	1.01	21.46	72	15.58	90
Pd-1b	CH <sub>3</sub>	Pd	(-5.11) <sup>EC</sup>	HTM	MAPbI <sub>3</sub>	FTO/SnO <sub>2</sub> /PCBM/perov./Pc/Au	P	1.06	21.08	73	16.28	90
Zn-16		Zn	(n/a)	HTM (+add.)	MAPbI <sub>3</sub>	FTO/cTiO <sub>2</sub> /mTiO <sub>2</sub> /perov./Pc/Au	m	16.35	0.797	50.3	6.7	91
Zn-17		Zn	(-5.26) <sup>EC</sup>	HTM (+add.)	(FAPbI <sub>3</sub> ) <sub>0.85</sub> (MAPbBr <sub>3</sub> ) <sub>0.15</sub>	FTO/cTiO <sub>2</sub> /mTiO <sub>2</sub> /perov./Pc/Au	m	17.52	0.890	46.52	7.25	92
Cu-17		Cu	(-5.35) <sup>EC</sup>	HTM (+add.)	(FAPbI <sub>3</sub> ) <sub>0.85</sub> (MAPbBr <sub>3</sub> ) <sub>0.15</sub>	FTO/cTiO <sub>2</sub> /mTiO <sub>2</sub> /perov./Pc/Au	m	19.01	0.870	50.56	8.33	92

<sup>a</sup>Abbreviations: **add.** = additives (usually LiTFSI and 4-*tert*butylpyridine); **cTiO<sub>2</sub>** = compact TiO<sub>2</sub> (blocking layer); **FA** = formylamidinium; **FTO** = fluorine doped tin oxide; **HTM** = hole transporting material; **MA** = methylammonium; **mTiO<sub>2</sub>** = mesoporous TiO<sub>2</sub>; **Pc** = Phthalocyanine; **perov.** = Perovskite; **PCBM** = 6,6-phenyl C<sub>61</sub> butyric acid methyl ester. <sup>b</sup>Work function (*W<sub>F</sub>*) of the Pc-HTL junction (EC: value estimated from electrochemical measurements in solution).



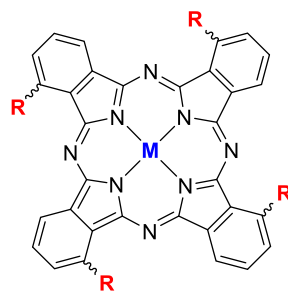
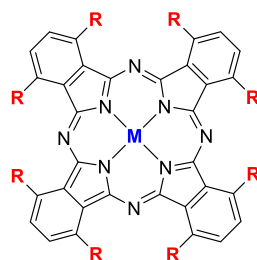


Fig. 4 General structures of  $\alpha$ -(tetrakis)substituted phthalocyanines (M = metal).

Table 4. Work function ( $W_F$ ) and role of  $\alpha$ -(tetrakis)substituted Pcs (see Fig. 4) employed in PSC, and photovoltaic performances of the champion devices under mesoporous (m) configuration.<sup>a</sup>

Pc	R =	M =	$W_F^b$ (eV)	Role	Perovskite composition	Architecture	Type	$J_{SC}$ (mA/cm <sup>2</sup> )	$V_{OC}$ (V)	F.F. (%)	PCE (%)	Ref
Cu-18		Cu	(-5.46) <sup>EC</sup>	HTM (+add.)	(FAPbI <sub>3</sub> ) <sub>0.75</sub> (MAPbBr <sub>3</sub> ) <sub>0.15</sub>	FTO/cTiO <sub>2</sub> /mTiO <sub>2</sub> /perov./Pc/Au	m	23.2	1.04	71	17.1	93
Cu-19		Cu	(-5.22) <sup>EC</sup>	HTM	(FAPbI <sub>3</sub> ) <sub>0.75</sub> (MAPbBr <sub>3</sub> ) <sub>0.15</sub>	FTO/cTiO <sub>2</sub> /mTiO <sub>2</sub> /perov./Pc/carbon	m	18.6	0.97	58	10.5	94
			(n/a)	HTM (6% doped- F4TCNQ)	(FAPbI <sub>3</sub> ) <sub>0.75</sub> (MAPbBr <sub>3</sub> ) <sub>0.15</sub>	FTO/cTiO <sub>2</sub> /mTiO <sub>2</sub> /perov./Pc/carbon	m	21.9	1.01	68	15.0	94

<sup>a</sup>Abbreviations: **add.** = additives (LiTFSI and 4-*tert*-butylpyridine); **cTiO<sub>2</sub>** = compact TiO<sub>2</sub> (blocking layer); **F4-TCNQ** = tetrafluorotetracyanoquinodimethane; **FA** = formylamidinium; **FTO** = fluorine doped tin oxide; **HTM** = hole transporting material; **MA** = methylammonium; **mTiO<sub>2</sub>** = mesoporous TiO<sub>2</sub>; **Pc** = phthalocyanine; **perov.** = perovskite. <sup>b</sup>Work function ( $W_F$ ) of the Pc-HTL junction (EC: value estimated from electrochemical measurements in solution; n/a: not reported).



**Fig. 5** General structures of  $\alpha$ -(octakis)substituted phthalocyanines (M = metal or 2H).

**Table 5.** Work function ( $W_F$ ) and role of  $\alpha$ -(octakis)substituted Pcs (see Fig. 5) employed in PSC, and photovoltaic performances of the champion devices under mesoporous (*m*) configuration.<sup>a</sup>

Pc	R =	M =	$W_F^b$ (eV)	Role	Perovskite composition	Architecture	Type	$J_{sc}$ (mA/cm <sup>2</sup> )	$V_{oc}$ (V)	F.F. (%)	PCE (%)	Ref
2H-20	<sup>n</sup> C <sub>5</sub> H <sub>11</sub>	2H	(-5.3) <sup>c,95</sup>	HTM (buff.)	MAPbI <sub>3</sub>	FTO/cTiO <sub>2</sub> /mTiO <sub>2</sub> /perov./Pc/MoOx/Au	<i>m</i>	18.8 <sup>av.</sup>	0.99 <sup>av.</sup>	55 <sup>av.</sup>	10.0 <sup>av.</sup> (12.2) <sup>best</sup>	96
Ni-21	O <sup>n</sup> Bu	Ni	(-5.06) <sup>EC</sup>	HTM	(FAPbI <sub>3</sub> ) <sub>0.85</sub> (MAPbBr <sub>3</sub> ) <sub>0.15</sub>	FTO/cTiO <sub>2</sub> /mTiO <sub>2</sub> /perov./Pc/Au	<i>m</i>	18.5	0.895	63.8	10.6	97
			(-5.06) <sup>EC</sup>	HTM (+add.)	(FAPbI <sub>3</sub> ) <sub>0.85</sub> (MAPbBr <sub>3</sub> ) <sub>0.15</sub>	FTO/cTiO <sub>2</sub> /mTiO <sub>2</sub> /perov./Pc/Au	<i>m</i>	23.0	1.070	72.8	17.9	97
			(-5.06) <sup>EC</sup>	HTM (buff.)	(FAPbI <sub>3</sub> ) <sub>0.85</sub> (MAPbBr <sub>3</sub> ) <sub>0.15</sub>	FTO/cTiO <sub>2</sub> /mTiO <sub>2</sub> /perov./Pc/V <sub>2</sub> O <sub>5</sub> /Au	<i>m</i>	23.1	1.080	73.4	18.3	97

<sup>a</sup>Abbreviations: **add.**: additives (LiTFSI and 4-*tert*butylpyridine); **buff.** = buffered; **cTiO<sub>2</sub>**: compact TiO<sub>2</sub> (blocking layer); **FA**: formylamidinium; **FTO**: fluorine doped tin oxide; **HTM**: hole transporting material; **MA**: methylammonium; **mTiO<sub>2</sub>** = mesoporous TiO<sub>2</sub>; **Pc**: phthalocyanine; **perov.**: perovskite; **PCMB**: 6,6-phenyl C<sub>61</sub> butyric acid methyl ester. <sup>b</sup>Work function ( $W_F$ ) of the Pc-HTL junction (EC: value estimated from electrochemical measurements in solution). <sup>c</sup>Value collected from ref 95 in the original article.

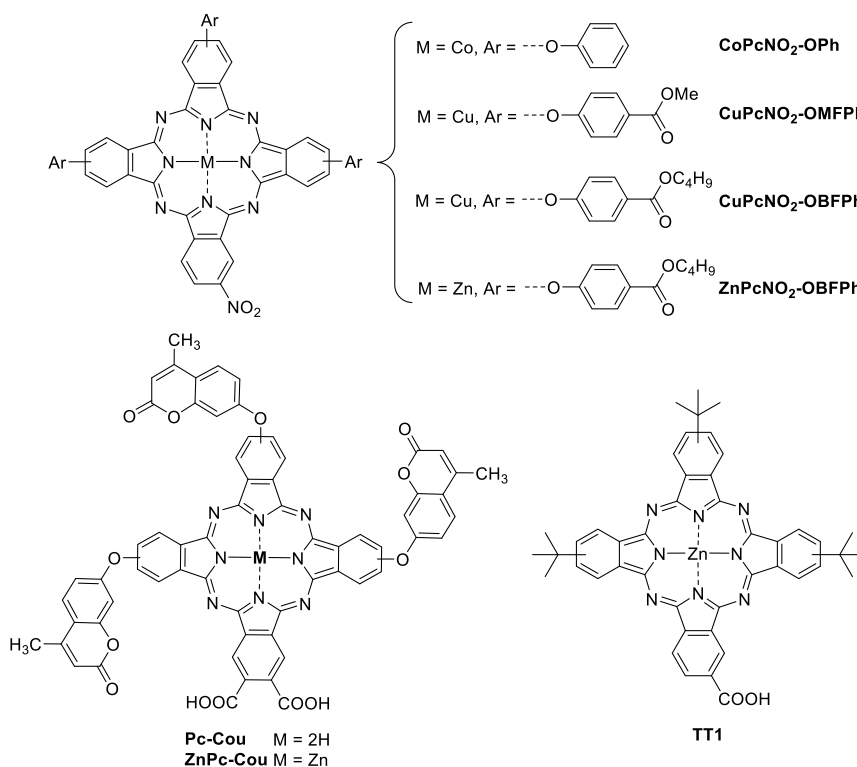


**Fig. 6** Molecular structures of unsymmetrically  $\beta$ -substituted Pcs.

**Table 6.** Work function ( $W_F$ ) and role of unsymmetrically  $\beta$ -substituted Pcs (see Fig. 6) employed in PSC, and photovoltaic performances of the champion devices under mesoporous (*m*) configuration.<sup>a</sup>

Pc	$W_F$ <sup>b</sup> (eV)	Role	Perovskite composition	Architecture	Type	$J_{sc}$ (mA/cm <sup>2</sup> )	$V_{oc}$ (V)	F.F. (%)	PCE (%)	Ref
TT1	(-5.44) <sup>EC</sup>	HTM (+add.)	FA <sub>0.1</sub> MA <sub>0.9</sub> PbI <sub>3</sub>	FTO/cTiO <sub>2</sub> /mTiO <sub>2</sub> /perov./Pc/Au	<i>m</i>	17.41	0.962	81.6	13.67	78
CoPcNO <sub>2</sub> -OPh	(-5.14) <sup>th</sup>	HTM	MAPbI <sub>3</sub>	FTO/cTiO <sub>2</sub> /mTiO <sub>2</sub> /perov./Pc/Au	<i>m</i>	11.79	1.04	64	8.24	98
CuPcNO <sub>2</sub> -OMFPh	(-4.98) <sup>EC</sup>	HTM	(FAI) <sub>0.85</sub> (PbI <sub>2</sub> ) <sub>0.85</sub> (MABr) <sub>0.15</sub> (PbBr <sub>2</sub> ) <sub>0.15</sub>	FTO/cTiO <sub>2</sub> /mTiO <sub>2</sub> /perov./Pc/Au	<i>m</i>	20.01	1.02	60	12.52	99
CuPcNO <sub>2</sub> -OBFPPh	(-4.96) <sup>EC</sup>	HTM	(FAI) <sub>0.85</sub> (PbI <sub>2</sub> ) <sub>0.85</sub> (MABr) <sub>0.15</sub> (PbBr <sub>2</sub> ) <sub>0.15</sub>	FTO/cTiO <sub>2</sub> /mTiO <sub>2</sub> /perov./Pc/Au	<i>m</i>	20.62	1.04	64	13.66	99
ZnPcNO <sub>2</sub> -OBFPPh	(-4.95) <sup>EC</sup>	HTM	(FAI) <sub>0.85</sub> (PbI <sub>2</sub> ) <sub>0.85</sub> (MABr) <sub>0.15</sub> (PbBr <sub>2</sub> ) <sub>0.15</sub>	FTO/cTiO <sub>2</sub> /mTiO <sub>2</sub> /perov./Pc/Au	<i>m</i>	21.00	1.10	68	15.74	99
Pc-Cou	(-5.56) <sup>th</sup>	Dye/ETM	MAPbI <sub>3</sub>	FTO/cTiO <sub>2</sub> /mTiO <sub>2</sub> +Pc/perov./Spiro/Au	<i>m</i>	21.42	0.926	68.45	13.55	100
ZnPc-Cou	(-5.52) <sup>th</sup>	Dye/ETM	MAPbI <sub>3</sub>	FTO/cTiO <sub>2</sub> /mTiO <sub>2</sub> +Pc/perov./Spiro/Au	<i>m</i>	22.53	0.919	67.44	13.96	100

<sup>a</sup>Abbreviations: add. = additives (LiTFSI and 4-*tert*butylpyridine); cTiO<sub>2</sub> = compact TiO<sub>2</sub> (blocking layer); ETM = electron transporting material; FA = formylamidinium; FTO = fluorine doped tin oxide; HTM = hole transporting material; MA = methylammonium; mTiO<sub>2</sub> = mesoporous TiO<sub>2</sub>; Pc = phthalocyanine; perov. = perovskite; Spiro = Spiro-OMeTAD (2,2',7,7'-tetrakis(*N,N'*-di-*p*-methoxyphenylamine)-9,9'-spirobifluorene). <sup>b</sup>Work function ( $W_F$ ) of the Pc-containing junction (EC: value estimated from electrochemical measurements in solutions; th.: value estimated from theoretical calculations).

## 2.1. Vacuum processed Pc-HTMs

**CuPc**, a low cost, robust and commercially available organic material, has been widely used as vacuum processed HTM (Table 1), and several works have reported on efficient and highly-stable PSCs using this material, under different configurations (*meso*, P and IP).<sup>44–54</sup> In *meso* configuration, Yang et al. reported a PSC device using dopant-free **CuPc** as HTM (under nanorod-like form) and a low-temperature processed carbon cathode, achieving an excellent maximum efficiency of 16.1%, comparable with that obtained for the control device made with the conventional (doped-) Spiro-OMeTAD as HTM and Au as back electrode.<sup>47</sup> Stability tests of the Pc-based devices conducted under one sun illumination, in ambient atmosphere, at room temperature and without encapsulation, showed excellent stability over 600h (Fig. 7). Later, Zhao and co-workers could improve this PCE value to 16.6% for a device within the same configuration (dopant-free **CuPc** and carbon counter electrode), in combination with a modified protocol for the preparation of high-quality perovskite film, a combined solvent and vapour treatment.<sup>46</sup> Turning to planar configurations, Ke et al. reported a fully-vacuum-processed PSC using **CuPc**-HTM (dopant-free) giving rise to 15.4% of efficiency, though expensive Au contact electrode and C<sub>60</sub> HTL were used in this study.<sup>48</sup> In a more recent work, Liu et al. could achieve the same efficiencies (15.4%) and excellent stability (over 1200 h; Fig. 8) using cheaper materials: a low-temperature printable carbon electrode and a planar-heterojunction TiO<sub>2</sub>/SnO<sub>2</sub> bilayer as ETL.<sup>51</sup> **CuPc** has also been implemented successfully as HTM in inverted (planar) PSCs. Two independent groups, those of Liao<sup>52</sup> and Wu,<sup>53</sup> have reported at the same time very similar structured inverted MAPbI<sub>3</sub>-based PSC devices using fullerene-BCP bilayers as ETL (PCBM and C<sub>60</sub>, respectively). Two different approaches have been considered to optimize the stability and performances of these devices.

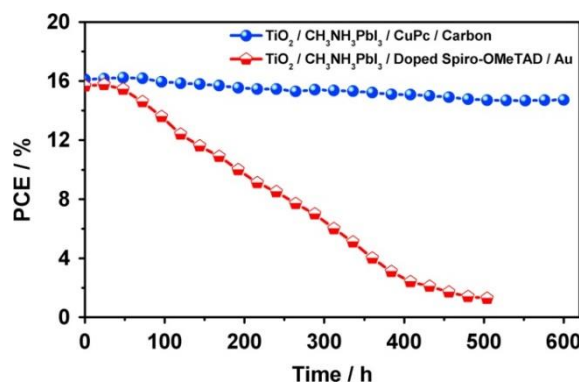


**Fig. 7** Stability tests of perovskite solar cells with **CuPc**/Carbon and doped-Spiro-OMeTAD/Au as HTMs and counter electrodes respectively. Reproduced with permission from ref 47. Copyright (2016) Elsevier

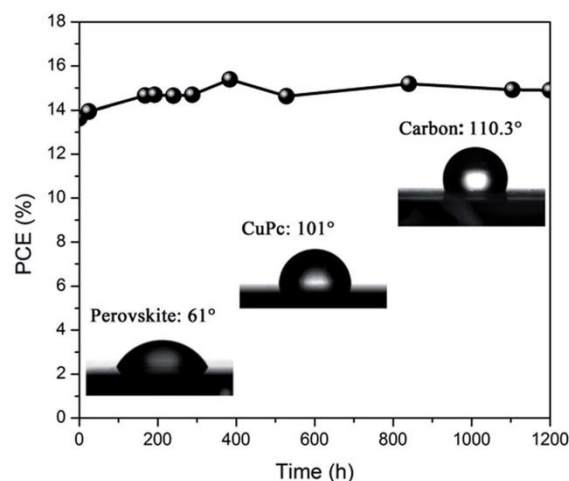


**Fig. 8** Long-term stability test without encapsulation (relative humidity, ~30%). The device was measured under 1 sunlight intensity, and kept in the dark until the next measurement. Inset: contact angle measurements of perovskite, CuPc and carbon films. Reproduced with permission from ref 51. Copyright (2018) Royal Society of Chemistry.

The former group used a triple-mixed cation modified perovskite ( $\text{Cs}_{0.05}\text{FA}_{0.81}\text{MA}_{0.14}$ ) instead of  $\text{MAPbI}_3$ , to achieve an improved 15.4% efficiency with respect to the  $\text{CuPc}/\text{MAPbI}_3$ -based device (14.5%).<sup>52</sup> The latter group inserted a thin layer of vanadium oxide ( $\text{VOx}$ ) between the ITO substrate and the  $\text{CuPc}$  (herein referred as “buffer layer”) to obtain a bi-hole layer, boosting the PCE of the modified device to 16.85% and with good moisture stability (only 10% efficiency loss after 350 hours in ambient air; Fig. 9).<sup>53</sup>

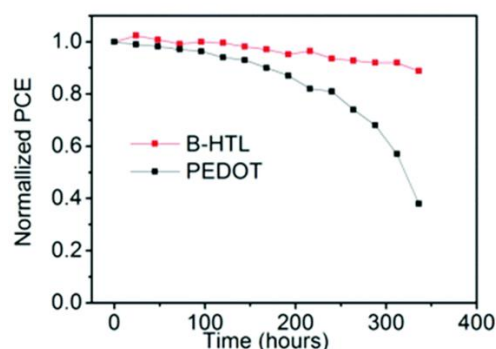


**Fig. 9** Normalised stability trends depicting the performances of the B-HTL ( $\text{Vox}/\text{CuPc}$ ) and PEDOT devices under ambient conditions with no encapsulation (40% relative humidity, RH). Reproduced with permission from ref 53. Copyright (2016) Royal Society of Chemistry.

The insertion of the  $\text{VOx}$  layer was found to be two-fold beneficial: 1) better charge extraction, and hence higher efficiency, was achieved owing to the alignment of the interfacial energy level with the  $\text{CuPc}$ , and 2) better stability of the device, owing to the synergic effect of the bi-HTM: the  $\text{VOx}$  inorganic material is stable and has good resistance toward corrosion, and the hydrophobic  $\text{CuPc}$  is excellent to protect the perovskite toward moisture decomposition. It should also be mentioned that the fabrication of the whole device involved low-temperature processes only, thus being beneficial for large-scale production, which, moreover, allowed for the fabrication of flexible PSC devices (on PET/ITO substrates) achieving an

excellent PCE of 14.4%.  $\text{ZnPc}$ , instead of  $\text{CuPc}$ , has also been envisaged, though in a lesser extent, in similarly structured PSC devices including *meso* (3.5%<sup>55</sup>), planar (16.8%,<sup>56</sup> 17.8%<sup>57</sup>), and inverted planar (11.6%)<sup>59</sup> configurations. Among them, Song, Dai, and co-workers reported on two successive works involving an innovative planar architecture, in which  $\text{ZnPc}$  is sandwiched between the perovskite and *Spiro*-OMeTAD layers of typical PSCs, acting as a buffer (or bi-layer) HTM that facilitates the hole transport between the two components and increase moisture-resistance.<sup>56,57</sup> In the first work,<sup>56</sup> a modified Nb-doped  $\text{TiOx}$  ETL was used as ETL, seeking to reduce electron recombination and photocurrent loss. Overall, the device incorporating the  $\text{ZnPc}$  extra layer showed improved PCE (16.8%) with respect to the control device without it (15.1%), and with high stability in ambient conditions, retaining 91% of the initial PCE after 2400 h (100 days) without encapsulation (Fig. 10a). In their second work,<sup>57</sup> a long-lasting photoluminescent SAED layer was introduced between the perovskite and compact  $\text{TiO}_2$  layers ( $\text{SAED} = \text{SrAl}_2\text{O}_4$  doped with  $\text{Eu}^{2+}$  and  $\text{Dy}^{3+}$ ). The SAED material has a broad and strong absorption in the UV region, and exhibits an emission in the green light region, in which the photoactive perovskite layer absorbs. The advantage is therefore two-fold: the SAED materials absorbs the high-energy UV-photons inhibiting UV degradation of the device, and convert them into green photons that the perovskite can absorb, improving the photovoltaic response. Moreover, it was found that the thermal activation energy of the trap states decreased from 109 to 63 meV in the presence of this layer, which is indicative of a contribution in the reduction of the recombination process. Given its influence on the light-induced trap states, the SAED layer was proposed to be also involved in the increase rate of self-healing. As the result, the device including this material showed an improved PCE of 17.8% with respect to the one without it (16.7%), and with a long-term stability (2600h at ambient atmosphere; Fig. 11). Apart from  $\text{CuPc}$  and  $\text{ZnPc}$ , other unsubstituted metal Pcs have also been envisaged as VD HTMs, namely  $\text{PbPc}$ ,<sup>55,60</sup>  $\text{Ti(O)Pc}$ ,<sup>61</sup>  $\text{V(O)Pc}$ ,<sup>62</sup> and  $\text{NiPc}$ <sup>63</sup> but gave low to modest results in comparison.

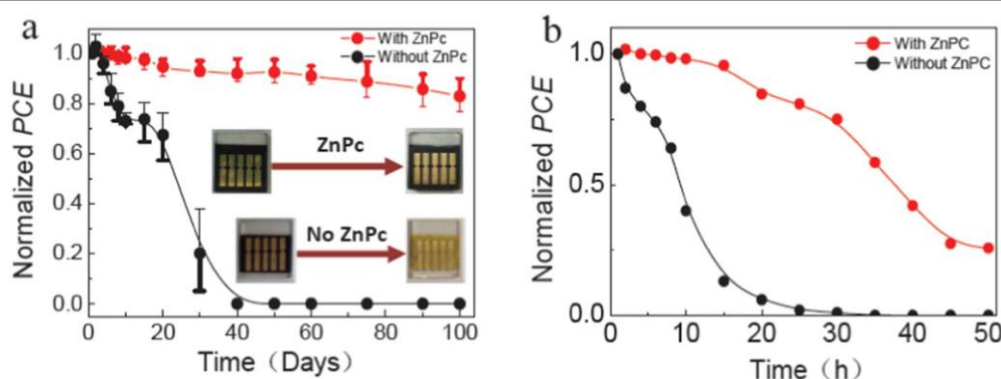


**Fig. 10** (a) Stability in ambient atmosphere of devices with and without  $\text{ZnPc}$  aging tests 2400 h, the inset shows the photographs of morphology change of two kinds of devices. (b) the stability of the two kinds of devices under the 75% RH condition. Reproduced with permission from ref 56. Copyright (2017) Elsevier.

## REVIEW ARTICLE

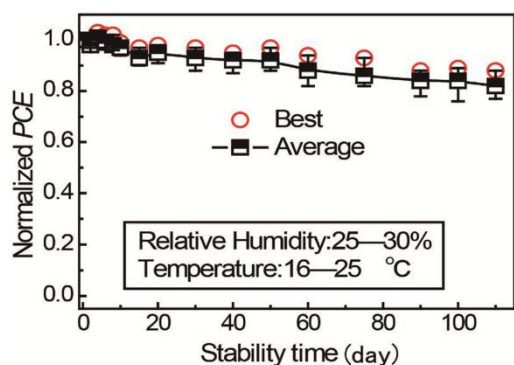


**Fig. 11** Stability of the devices (using **ZnPc** as a bi-HTM buffer) in an ambient environment without encapsulation. The relative humidity was controlled to be 25–30%. The temperature in the atmosphere was controlled to be 16–25 °C. Reproduced with permission from ref 57. Copyright (2017) Wiley.

A step further came with the functionalization of the Pc macrocycle with short methyl or ethyl chains at the peripheral  $\beta$ -positions, including  $\beta$ -tetrakis (**Cu-1a**,<sup>49,65</sup> **Cu-2**,<sup>49</sup> Table 2) and  $\beta$ -octakis substitution patterns (**2H-1b**,<sup>89</sup> **Zn-1b**,<sup>89</sup> **Cu-1b**<sup>50,90</sup> and **Pd-1b**<sup>90</sup>; Table 3), which were also successfully implemented in PSCs as vacuum-processed HTMs.

On this line, Xu et al. reported an interesting comparative study between two  $\beta$ -tetraalkyl substituted Pcs (**Cu-1a**, R = Me and **Cu-2**, R = Et) and the unsubstituted **CuPc** as VD-HTMs in planar PSCs, which achieved maximum PCEs of 11.9%, 11.7% and 9.1%, respectively.<sup>49</sup> The hole mobility values determined from the OFET-films, increased in the order **CuPc** < **Cu-2** (Et) < **Cu-1a** (Me) ( $\mu_{\text{FET}}$  = 1.8, 3.8, and 6.1 [ $\times 10^{-4}$  cm<sup>2</sup>·V<sup>-1</sup>·s<sup>-1</sup>], respectively). On the other hand, space-charge limited current (SCLC) mobility measurements also gave the highest value for **Cu-1a** ( $\mu_{\text{SCLC}}$  = 19.5  $\times 10^{-4}$  cm<sup>2</sup>/Vs) but in turn, that of **Cu-2** (3.75  $\times 10^{-4}$ ) was found to be lower than **CuPc** (7.45  $\times 10^{-4}$ ). XRD and AFM experiments conducted on the thin films evidenced more tightly-packed and ordered structures for the alkyl-substituted Pc-films. Thus, it was concluded that the presence of the alkyl substituents favour  $\pi$ - $\pi$  stack arrangements of these macrocycles during the VD process, which was accounted for their higher hole mobility values and, accordingly, superior PCEs. The differences between **Cu-1a** and **Cu-2** was ascribed to shorter  $\pi$ - $\pi$  stacking distances for the former owing to the smaller size of methyl than ethyl substituents.

Along the same lines, some important insights were further provided by Xu, Fang et al. with a fully substituted analogue, the  $\beta$ -octamethyl copper Pc (**Cu-1b**).<sup>50</sup> In planar PSCs, a 25% improvement in the PCE was obtained with the VD-HTM **Cu-1b** (15.73%) with respect to the unsubstituted one, **CuPc** (12.55%). As well, they found that the **Cu-1b** film displayed a more

condensed structure and higher hole mobility than pristine **CuPc** by two orders of magnitude ( $\mu$  = 4.79  $\times 10^{-2}$  and 7.25  $\times 10^{-4}$  cm<sup>2</sup>/Vs, respectively), accounting for its superior efficiency. Grazing incidence X-ray diffraction (GIXRD) experiments were performed of the thin film samples deposited on FTO surface, with and without the perovskite layer. In the absence of the perovskite layer, both Pcs adopt an edge-to-face (*i.e.*: perpendicular) orientation to the surface. However, when the perovskite is present, **Cu-1b** adopts a face-to-face (parallel) orientation, whereas the normal orientation of unsubstituted **CuPc** remains unchanged (edge-to-face). Therefore, it was unravelled that the reason behind the higher hole mobility of **Cu-1b** was coming from the planar orientation of the  $\pi$ - $\pi$  stacks on the perovskite surface, facilitating a vertical charge transport. Again, the PSCs made with hydrophobic HTM **Cu-1b** showed excellent resistance to moisture, as well as long-term stability, retaining 95% of the initial efficiencies after 2000h at ambient atmosphere (Fig. 12; with “**CuMe<sub>2</sub>Pc**” = **Cu-1b**).

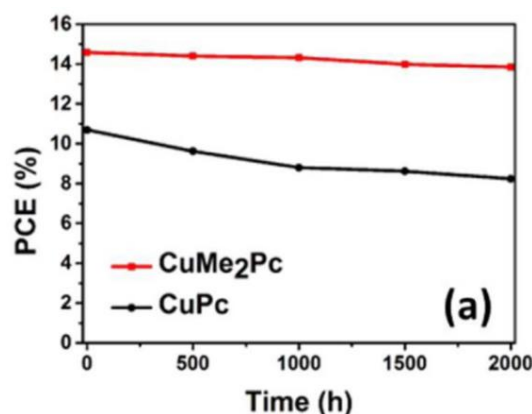


**Fig. 12** PCE values as a function of ambient storage time of the devices with different hole conductor (with “**CuMe<sub>2</sub>Pc**” = **Cu-1b**). Reproduced with permission from ref 50. Copyright (2017) Elsevier

The same collaborators further reported a palladium-Pc analogue (**Pd-1b**) with improved efficiency in planar PSC with respect to **Cu-1b**, previously reported.<sup>90</sup> In that case too, **Pd-1b** presented a face-to-face orientation (evidenced by GIXRD experiments). Palladium, with a heavier atom effect than copper, strengthens the spin–orbit coupling thus enhancing the singlet-to-triplet excitons. In principle, this property should not be beneficial for photovoltaic applications since long-lived triplet carriers tend to have low mobilities. Nonetheless, **Pd-1b** device did not experiment any significant decrease in terms of conductivity, and in fact only slightly lower value was obtained with respect to **Cu-1b** (3.42  $\times 10^{-2}$  and 4.79  $\times 10^{-2}$  cm<sup>2</sup>/Vs,

respectively). As counterpart, much longer carrier lifetimes for Pd-**1b** than Cu-**1b** layer (7.7 ns vs 3.4 ns) were deduced from transient absorption (TA) spectroscopy experiments, which is traduced by longer diffusion length of excitons (26 nm vs 20 nm), and hence lower charge recombination rates. Consequently, Pd-**1b**/PSC displayed improved PCE (16.28%) with respect to Cu-**1b** (15.58%), and with better moisture stability (stressed from 40% to 100% of relative humidity conditions). Under ambient atmosphere, the Pd-**1b** device maintained 96% of its initial performance after 600 h (Fig. 13).

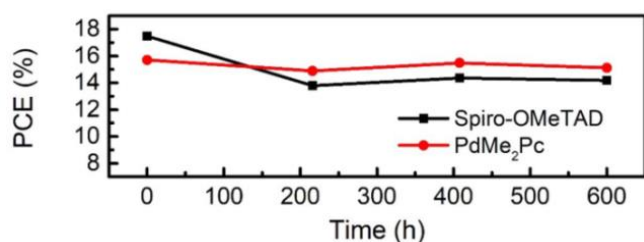


Fig. 13 Long-term stability of the PSCs with PbMe<sub>2</sub>Pc (red circle) and Spiro-OMeTAD (black square) HSLs (with "PdMe<sub>2</sub>Pc" = Pd-**1b**). Reproduced from the Supplementary Information with permission from ref 90. Copyright (2017) Elsevier.

The same collaborators further reported other two octamethyl-substituted analogues as HTMs of planar PSCs, namely a zinc (Zn-**1b**) and metal-free (2H-**1b**) Pcs, to shed light on the effect of the metal centre.<sup>89</sup> Obviously, metal-free Pcs being pure organic materials, circumvent issues encountered with the use of most of the metals (contamination, rarity and extra cost) thus holding a main advantage over their metal-Pc analogues for commercial applications. Free-base Pcs present several differences in terms of optical and electrochemical properties with respect to their metallic analogues, thus affecting their HOMO-LUMO band gap, in particular. Accordingly, 2H-**1b** presents a smaller band gap and less favourable alignment than Zn-**1b** of its energetic levels with respect to the perovskite and Au electrode. Nonetheless, 2H-**1b** film displays higher hole-mobility ( $2.72 \times 10^{-2} \text{ cm}^2/\text{Vs}$ ) than Zn-**1b** ( $1.80 \times 10^{-2}$ ), accounting for their differences in PCEs (15.59% vs 14.88%). In these cases too, GIXRD experiments evidenced a face-to-face (parallel) orientation for both HTMs, responsible of their excellent conductivity. In terms of stability 2H-**1b** device exhibited superior performances too, with a 2.2% decrease in the PCE after 10 days under a relative humidity of 70% (at 25 °C, and without encapsulation), compared with Zn-**1a** (6.4% decrease; Fig. 14 with "HMe<sub>2</sub>Pc" = 2H-**1b** and "ZnMe<sub>2</sub>Pc" = Zn-**1b**).

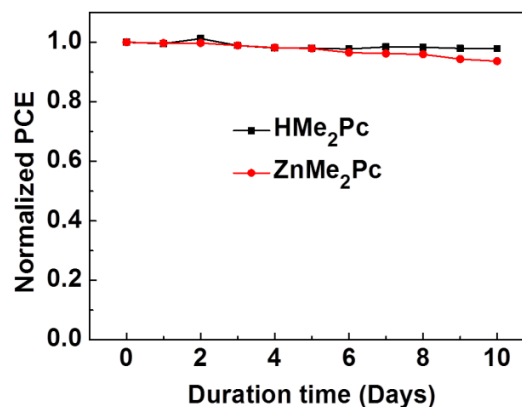


Fig. 14 Normalized PCE degradation of perovskite solar cells based on Pc HTMs (25 °C and a relative humidity of 70%); with "HMe<sub>2</sub>Pc" = 2H-**1b** and "ZnMe<sub>2</sub>Pc" = Zn-**1b**. Reproduced from the Supplementary Information with permission from ref 89. Copyright (2018) Elsevier.

## 2.2. Solution processed Pc-HTMs

### 2.2.1. Alkyl and alkoxy substituted Pcs.

$\beta$ -tetrakis substituted MPcs with longer/bulkier alkyl chains (n-propyl, n-butyl, *tert*-butyl) have been used as solution-processed (SP) HTMs. A first remarkable example came with the  $\beta$ -tetrapropyl Cu-Pc (Cu-**3**) reported by Xu et al., used as a dopant-free HTM in planar (SnO<sub>2</sub>)-PSC.<sup>66</sup> Interestingly, GIXRD experiments also evidenced a face-to-face orientation for this SP-Pc, similarly than various VD-CuPcs discussed in the previous section (substituted with shorter Me or Et chains). Excellent stability (Fig. 15) and high PCEs with an average value of  $17.0 \pm 0.5$  % (max. 17.8%), were achieved with this solution-processed and dopant-free HTM.

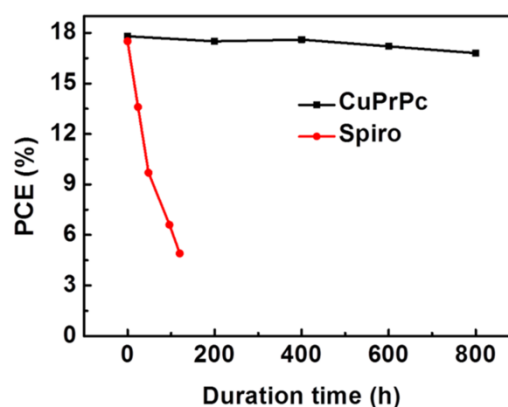


Fig. 15 Long-term stability of the PSCs with CuPrPc and Spiro-OMeTAD at 25 °C with relative humidity of 75% without any encapsulations (with "CuPrPc" = Cu-**3**). Reproduced with permission from ref 66. Copyright (2018) Wiley.



The longer butyl version Cu-4 ( $\beta$ -tetra-*n*-butyl- CuPc), was reported by various groups in *meso*-type PSC, with efficiencies ranging from 7.3%–15.9%.<sup>67–69</sup> Lianos and co-workers obtained a modest PCE for the devices made solely with this Pc-HTL (7.3%), but could be significantly increased by incorporating either Al<sub>2</sub>O<sub>3</sub> (9.7%) or graphene oxide (14.4%) buffer layers between the perovskite and Pc layers.<sup>67</sup> The authors suggested that the presence of defects (voids) in the non-uniform and aggregated structure of the Pc-films could constitute a possible explanation for the low performances obtained with the neat HTM. The buffer layer (GO or Al<sub>2</sub>O<sub>3</sub>) should fill these voids, thus repairing the defective sites of the film. It must be remarked that additives (TBP and Li-TFSI) were incorporated in the Pc precursor solution for the fabrication of the HTL layer. In a later work, the same collaborators improved further the efficiency and stability (Fig. 16) of their GO(buffered)/Cu-4 PSC devices by using a modified and *in situ* prepared mesoporous layer (ETL contact), consisting of mesoporous TiO<sub>2</sub> particles doped with reduced graphene oxide (RGO; 0.2 wt%), rising significantly the efficiency up to 15.9%.<sup>68</sup> This improvement was ascribed to two main factors owing to the presence of RGO in the mesoporous layer: 1) it confers higher porosity of the TiO<sub>2</sub>, thus providing a better penetration of the perovskite in it; and 2) it reduces charge recombination. The bulkier  $\beta$ -tetra(*tert*-butyl) version (Cu-5 and Zn-5) has also been largely investigated, which stands out for reduced aggregation (and hence improved solubility) with respect to Cu-4 (with linear *n*-butyl chains).<sup>69,71–74</sup> On this line, an interesting comparative study between  $\beta$ -tetra(*n*-butyl) (Cu-4) and  $\beta$ -tetra(*tert*-butyl) (Cu-5) CuPcs was reported by the same collaborators, to shed light on the importance of  $\pi$ - $\pi$  stacking aggregation of Pc toward molecular ordering and efficiency.<sup>69</sup> Cu-4 displayed stronger aggregation than Cu-5 as supported by UV-vis spectrum in solution. GIXRD analysis evidenced, as expected, higher crystallinity for the Cu-4 than Cu-5 films, together with a more compact structure. Drastic differences in the carrier mobility values were found for the Pc-based OFET films, that of Cu-4 being almost 40 times higher than that of Cu-5 ( $5.0 \times 10^{-5}$  and  $1.3 \times 10^{-6}$  cm<sup>2</sup>·V<sup>-1</sup>·s<sup>-1</sup>), which was explained in terms of a better packing and stronger  $\pi$ - $\pi$  interaction of the former. Consequently, the device made with HTM Cu-4 achieved larger  $J_{SC}$ , which mostly account for its superior PCE (8.5% vs 6.5%). Seo, Seak, and co-workers have successively used Cu-5 as HTM in *meso*-type PSCs devices with improved efficiencies of up to 15.2% and 18.8%, using a double mixed cation (FA/MA) perovskite. In the later work, stability tests were also performed on the Cu-5/PSC devices, which maintained 97% of their initial efficiencies for more than 1000 h at 85°C and under 25–30% of relative humidity (Fig. 17; with “CuPc” = Cu-5).<sup>72</sup>

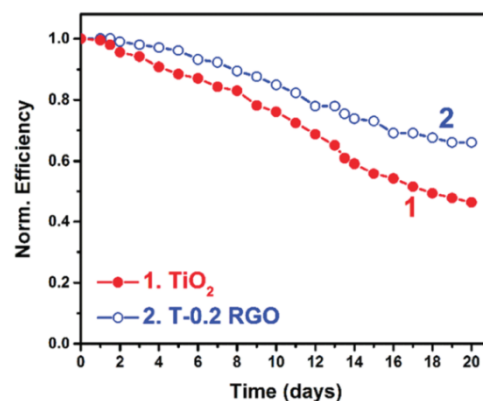


Fig. 16 Normalized efficiency as a function of ageing time for mesoscopic PSC devices based on (1) pure TiO<sub>2</sub> and (2) T/0.2RGO mesoporous layers as electron transport mediators. Reproduced from ref 68 Copyright (2018) with permission from the PCCP Owner Societies.

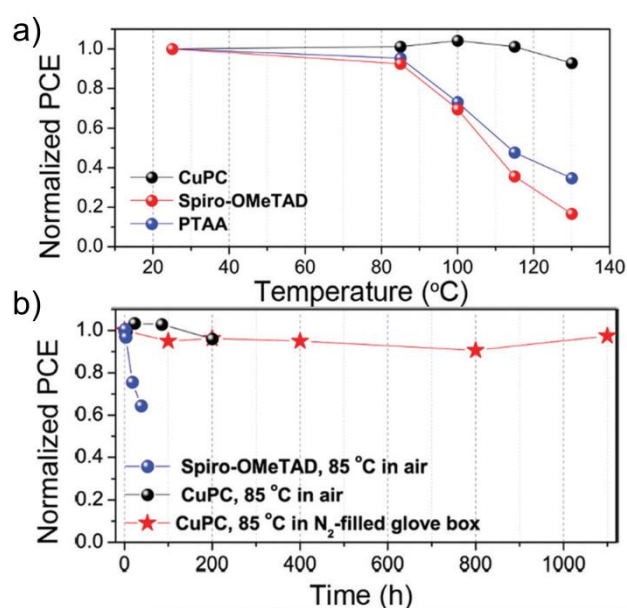


Fig. 17 Stability of the devices stressed at different temperatures (25, 85, 100, 115 and 130 °C, respectively) for 30 min, employing CuPC (black color), spiro-OMeTAD (red color), and PTAA (blue color). (b) Long-term stability of the devices stressed at 85 °C in air (25–30% humidity), employing FAPbI<sub>3</sub>/CuPC (black color) and FAPbI<sub>3</sub>/spiro-OMeTAD (blue color). 1100 h stability of the device utilizing FAPbI<sub>3</sub>/CuPC at 85 °C in a nitrogen-filled glove box (red color). (with “CuPc” = Cu-5). Reproduced with permission from ref 72 Copyright (2018) Royal Society of Chemistry.



At the same time, the groups of Duong and Catchpole improved further this PCE of up to 20.1%, using a modified quadruplication (Cs/Rb/FA/MA) mixed perovskite, together with a thermal post-treatment during the fabrication of the HTM.<sup>73</sup> Interestingly, and in agreement with the observations and conclusions reported by Lianos and co-workers for the analogue Cu-**4** discussed previously (*vide infra*),<sup>67</sup> many cracks were observed on the Pc-film surface, exposing the perovskite to a direct contact with the Au electrode. These defects make shunts and thus increase recombination processes at the interfaces. Fortunately, the authors discovered that these defects could be greatly reduced by a subsequent thermal post-treatment at 85 °C (optimized temperature) after deposition of the Au layer on top of it. It was proposed that the Au particles rearrange and migrate from the cracks to form much bigger particles, passivating the defects and, in a lesser extent, also act as dopant of the HTM. It is important to remark that, in these three last works, Li-TFSI and TBP additives were also incorporated in the Pc precursor solution for the fabrication of the HTL.

In a different context, longer n-pentyl and alkoxy chains (linear n-BuO or branched 2,4-dimethyl-3-pentoxo) have been used in  $\alpha$ -substituted Pcs Cu-**18**,<sup>93</sup> **20**,<sup>96</sup> and Ni-**21**,<sup>97</sup> and although scarcely considered, very good efficiencies could be obtained with this class of Pc-HTM in *meso*-type PSCs (Figs. 4, Table 5). Importantly, these Pcs are known to present a more distorted macrocycle with respect to their  $\beta$ -analogues, which strongly impacts on their intrinsic properties (topological, optical, electrochemical and energetics), and importantly, also on their aggregation behaviour.<sup>101,102</sup> Dao et al. reported on an  $\alpha$ -octa(n-pentyl) substituted Pc (**2H-20**; Fig. 5 and Table 5), as a metal- and dopant-free HTM in *meso*-type PSC,<sup>96</sup> and in agreement with the findings of Seo, Seak,<sup>73</sup> previously discussed (see above), the authors also found that a thermal annealing of the Pc-films was beneficial in terms of stability and performances of the devices. By thermal-annealing under optimal conditions (130 °C, 10 min) the performances of the PSCs were greatly improved (average PCE of 10.0%, max. 12.2%) with respect to the devices without this post-treatment (average PCEs of 6.1%), which they ascribed to better charge carrier mobility. It has to be remarked that a thin layer of MoOx was deposited on top of the HTL and before Au deposition for the fabrication of the devices, and though not commented by the authors in the article, this buffer MoOx layer might play an important role in reducing recombination (see hereafter). Similarly, Sun and co-workers reported an integrated HTL based on an  $\alpha$ -octa(n-butyloxy) substituted Pc (Ni-**21**) and vanadium oxide for *meso*-type PSCs.<sup>97</sup> When the HTL layer was fabricated with Ni-**21** solely (from 30 mg/ml solutions) and without dopant, a relatively poor efficiency of 10.6% was obtained. SEM images revealed, once again, incomplete coverage of the perovskite layer by the Pc film. When the concentration was increased to 50 mg/ml, thicker films were obtained that fully covered the perovskite, but the performances still remained low (especially fill factor). For these thick films, the use of dopants (Li-TFSI and TPB) was necessary to improve their conductivity, and indeed, excellent efficiencies with average values of 17% were obtained under these conditions (max.

17.9%). Another strategy was to introduce a buffer layer (V<sub>2</sub>O<sub>5</sub>) on top on the Pc-layer, covering the defects encountered during the fabrication of the thin-films, hence reducing recombination losses. No perovskite crystals and only the compact V<sub>2</sub>O<sub>5</sub> sheet could be detected by SEM, confirming the success of this strategy. It also presents the advantage to make the use of dopant useless, since the thin film itself shows high conductivity. In this way, the PSC devices made with the dopant-free V<sub>2</sub>O<sub>5</sub>/Ni-**21** modified layer achieved improved PCEs with average values of 17.6% (max. 18.3%) and excellent stability over 30 days (Fig. 18).

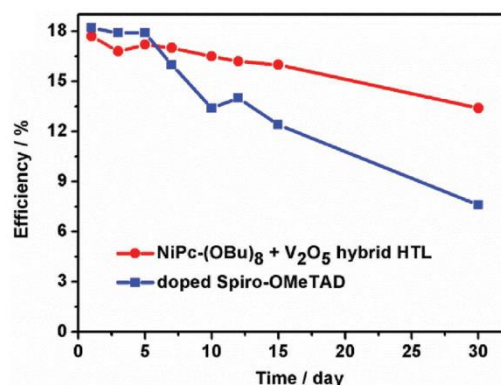


**Fig. 18** Shelf stability of unencapsulated PSCs under dark ambient conditions (humidity about 40%–45% and temperature of 20–25 °C); with NiPc-(OBU)<sub>8</sub> = Ni-**21**. Reproduced with permission from ref. 97 Copyright Wiley (2017).

### 2.2.2. Aryl and heteroaryl substituted Pc-HTMs

More elaborated substituents than simple alkyl or alkoxy chains have also been sought for Pc materials. Back in 2015, the groups of Torres and Nazeeruddin reported one of the first examples of a substituted and solution-processed Pc-based HTM in PSC, with the Zn(II)octa(2,6-diphenylphenoxy) Pc Zn-**16** (coded as **TT80**).<sup>91</sup> The authors demonstrated earlier in a different context that this substitution pattern fully suppress aggregation of the Pc, whereas it was not the case for a *tert*-butyl substitution. This breakthrough was successfully implemented by these authors in the dyes **TT40** and **TT58** for DSSC applications, giving rise to one of the most efficient Pc-sensitizers to date.<sup>103,104</sup> For HTM Pcs, however, the opposite aggregation-efficiency relationship was observed in PSCs, with the non-aggregated Zn-**16** (doped) giving rise to a PCE of 6.7%, whereas the (more aggregated) *tert*-butyl-substituted analogue Zn-**5** (doped), reported some years later by the same authors, achieved much higher efficiencies of successively 13.3%<sup>77</sup> (max. 14.48%) and 13.7% (max. 14.0%)<sup>78</sup> (dopants Li-TFSI and TBP were used in the three works). Though different perovskite materials were used in these three studies, the abysmal differences in efficiency between the two HTMs cannot be explained by this factor but, instead, in terms of conductivity and morphology of the Pc-films which, as discussed before, emphasizes the critical importance of  $\pi$ - $\pi$  stacking for such application. Similar results were obtained by Sastre-Santos and

co-workers for the  $\beta$ -octakis substituted Pcs Zn-17 and Cu-17 tethered with bulky alkylphenoxy groups, achieving PCEs of 7.25% and 8.25%, respectively, within the same device configuration and using, as well, Li-TFSI and TBP dopants.<sup>92</sup> Zhang and co-workers reported two coumarine-based metal Pcs, Fe-7 and Ni-7, which despite the remarkable hole mobility of the corresponding films ( $3.65 \times 10^{-6}$  and  $4.78 \times 10^{-6} \text{ cm}^2 \text{ V}^{-1} \text{ s}^{-1}$ , respectively), achieved modest PCEs of 9.40% and 10.23% in PSCs.

In a broader context, triarylamine (TPA)-based small molecules or polymers, stand out as high-performing HTMs for photovoltaic applications, including PSCs, such as the well-known poly(triarylamine) (PTAA).<sup>105–107</sup> On this line, the groups of Giribabu and Lianos reported the Pc Zn-8, substituted with four peripheral TPA groups, but again low PCEs in the range of 5.6% to 9.0% were obtained for the devices made with this HTM, and Li-TFSI and TBP dopants were necessary as well. An additional  $\text{Al}_2\text{O}_3$  buffer layer on top of the HTM layer could improve the PCE to a better but still quite modest value of 13.65%, which suggests not only issues from conductivity of the Pc-films themselves but also defects and/or non-homogeneity of the Pc-film, as discussed previously. One more successful example involved an  $\alpha$ -type Pc-HTM Cu-19, functionalized with 4-(bis(4-*tert*-butylphenyl)amino)phenoxy substituents.<sup>94</sup> Cu-19 was tested in double-cation (FA/MA) mixed PSC, but it firstly achieved as well low PCEs, with a maximum value of 10.5%, the main reason being the relatively low conductivity of this HTM ( $5 \times 10^{-7} \text{ S cm}^{-1}$ ). To improve the conductivity and performances, the authors focused their attention on tetrafluoro-tetracyanoquinodimethane (F4TCNQ) as p-dopant. This choice was first motivated by the good alignment of the LUMO level of F4TCNQ (-5.24 eV) with the HOMO of Cu-19 (-5.22 eV), which is favourable for an efficient electron transfer from the Pc to F4TCNQ, with the aim to increase the conductivity of the HTM (so-called p-doping). Another advantage of F4TCNQ is to avoid common dopants such as Li-TFSI, which, given its high hygroscopic nature, may accelerate the degradation of cells involving solid state HTMs, as proposed by studies related to other photovoltaic technologies.<sup>108,109</sup> p-Doping of Cu-19 with 6% (w/w) of F4TCNQ increased almost 18 times the conductivity of the films (from  $5 \times 10^{-7}$  to  $8.9 \times 10^{-6} \text{ S cm}^{-1}$ ). Accordingly, the optimized device using the doped-HTM achieved a considerably improved PCE of 15.0%, which is a relatively high value considering that a low-cost carbon counter electrode was used in this study. The PSC devices showed good stability under ambient condition for 720 h (Fig. 19). The groups of Pozzi and Nazerrudin reported on Pcs substituted with secondary amine donor groups, including diphenylamine (Zn-9) and carbazole (Zn-10 and Zn-11), which stand out for the direct N-bonding to the Pc macrocycle.<sup>83</sup> As one could expect, these strong  $\pi$ -donor groups directly connected to the macrocycle produced drastic changes in their optical and electrochemical properties (thus HOMO-LUMO levels) with respect to non-conjugated alkyl/aryl or alkoxy/phenoxy-type Pcs discussed before (*vide supra*). In particular, these new ZnPcs have lower LUMO energy, smaller bandgap, and redshifted Q-band absorption, than other ZnPcs. The diphenylamino-substituted Pc Zn-9 showed higher HOMO

level (-4.96 eV) than its carbazole analogue Zn-10 (-5.39 eV). The introduction of methoxy donor groups in Zn-11 limited the stabilizing effect produced by the carbazole unit on the HOMO level, thus having an intermediate value of -5.18 eV. Overall, it was expected enough over-potential for the three Pcs for a favourable hole extraction from the perovskite ( $\text{MAPbI}_3$ ; -5.48 eV). The LUMO energy increased in the order Zn-10 (-3.57 eV) < Zn-11 (-3.39 eV) < Zn-9 (-3.24 eV), which confer greater over-potential for blocking the backflows of electron from the perovskite to the Pc, and hence recombination can be expected to be reduced in the same order. These data are consistent with the poor photocurrent observed for Zn-10/PSC ( $J_{\text{SC}} = 10.7 \text{ mA cm}^{-2}$ ) in comparison with the two other devices ( $J_{\text{SC}} = 16.7$  and  $17.4 \text{ mA cm}^{-2}$  for Zn-9 and Zn-11, respectively). Accordingly, the device made with Zn-10 achieved a PCE of 6.65% only, while those of Zn-9 and Zn-11 achieved comparable efficiencies of 11.75% and 11.44% respectively, which at that time, were the highest values ever reported for solution-processed Pcs in conventional PSCs. The relative and modest efficiencies achieved with these Pc-HTMs in PSCs can be well-explained by energetic factors, which are misalignments of their HOMO-LUMO levels with the energy band edges of the perovskite material. The group of Nazeeruddin also reported on the use of alkyl-thiophene and -bisthiophene moieties to produce low band gap Pc-materials. Their first attempt came with the tetra- $\beta$ -hexylthiophene-substituted Pc (Zn-12) in  $\text{MAPbI}_3$ -based PSCs.<sup>84</sup> Initially, they found efficiencies as poor as 4.2% for this HTM, which were ascribed to the low quality of the films (large defects and shunts), hence resulting in high recombination rates. To solve this critical issue, the authors developed an innovative strategy that consists in infiltrating the Pc film with insulating  $\text{Al}_2\text{O}_3$  mesoporous particles to form a hybrid interfacial buffer layer. Charge recombination was greatly reduced upon incorporation of the  $\text{Al}_2\text{O}_3$  interlayer, resulting in an impressive improvement in the PCE of up to 12.3%.

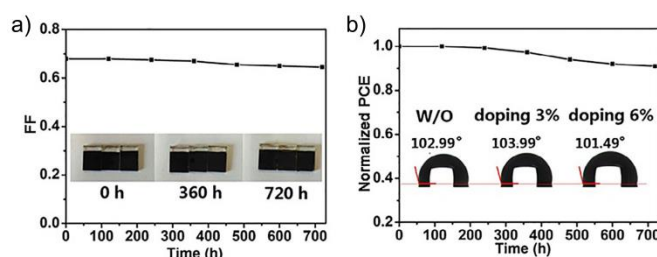


**Fig. 19** Stability tests for PSC devices based on CuPc-OTPAAtBu as HTMs. The devices without encapsulations were stored at ambient conditions in the dark at room temperatures with a humidity of approximately 30% measured under 100  $\text{mW cm}^{-2}$  illumination (AM 1.5G). Evolution of a) F.F. vs Time and b) PCE vs time; with "CuPc-OTPAAtBu" = Cu-19. Reproduced with permission from ref 94. Copyright Wiley (2017).

In a later work,<sup>77</sup> this Pc together with other two, Zn-5 and Zn-13 having a *tert*-butyl or hexylbisthiophene substitution, respectively, were explored in PSCs using a modified double-cation, double-halide, mixed perovskite [ $\text{FAPbI}_3$ ]<sub>0.85</sub>( $\text{MAPbBr}_3$ )<sub>0.15</sub>], distinguished by a sharper optical

bandgap than  $\text{MAPbI}_3$ , which is optimal for solar cell applications.<sup>110</sup> The three Pc-HTMs reached comparable  $J_{\text{sc}}$  (20.2–20.3  $\text{mA}\cdot\text{cm}^{-2}$ ) and  $V_{\text{oc}}$  (1.03–1.10 V) values, but with remarkable differences in their FF. Indeed, Zn-12 achieved record FF values up to 0.803, while those of Zn-5 (0.663) and Zn-13 (0.694) were low in comparison. Accordingly, Zn-12 yielded a record PCE of up to 17.5%, while more modest values were obtained for Zn-5 (up to 14.5%) and Zn-13 (up to 15.5%). The difference in PCEs of the three HTMs was related to morphology considerations and degree of stacking of the Pcs, which was corroborated by conductivity measurements of the films. Zn-5 and Zn-13 displayed the lowest values of  $6.0\times 10^{-7}$  and  $5.0\times 10^{-7}$   $\text{S}\cdot\text{cm}^{-1}$ , respectively. In turn, Zn-12 films showed impressive values higher by two orders of magnitude ( $8.0\times 10^{-5}$   $\text{S}\cdot\text{cm}^{-1}$ ) with respect to the other Pcs, and comparable to that of the conventional *Spiro*-OMeTAD HTM ( $4.0\times 10^{-5}$   $\text{S}\cdot\text{cm}^{-1}$ ). This trend, once again, clearly supports that an optimal packing through  $\pi$ - $\pi$  stacking of Zn-12 has a crucial importance on the conductivity of the Pc-films.

### 2.2.3. Other Pc-HTMs

The copper Pc Cu-6 reported by Sun and collaborators,<sup>79</sup> is distinguished by the introduction of four triisopropylsilyl ethynyl (TIPS) groups at the periphery of the Pc, affording good solubility and greater hydrophobicity, which aims to allow solution-process and greater stability of the final devices, with respect to the commonly used, vacuum-processed unsubstituted CuPc HTM. PSCs fabricated with HTM Cu-6 achieved a PCE of up to 14%, a decent value taking into account that the HTM was solution-processed and dopant-free, and a more stable, low-cost carbon counter electrode was used in this study, which together, aim to reduce the fabrication costs and enhance long-term stability of the device. It is worth to remark that Cu-6 films with no dopant showed a good conductivity value of  $5\times 10^{-6}$   $\text{S}\cdot\text{cm}^{-1}$ . The Cu-6/PSC devices showed good stability over 30 days under a humidity of 35%, without encapsulation and stored in the dark (Fig. 20), retaining 90% of the initial PCE (from 14% to 12.5%). A last example concerns a cationic  $\beta$ -tetrasulfonated acid tetra sodium salt Pc reported by two independent groups but with different metal centres (Cu-14<sup>85,86</sup> or Ni-14<sup>87</sup>), in planar-PSCs, under normal and/or inverted configurations. Solely and dopant-free, these cationic Pc-HTMs gave relatively poor-to-modest PCEs, which was ascribed mostly to low conductivity and hole mobility of the Pc films, as well as non-uniformity when formed over the ITO glass substrate for inverted PSC. Dopant or doping approaches were developed to engineer new composite HTLs based on these Pcs, with the aim to improve efficiency and stability of the PSC devices.

The work reported by Wang et al. relied on p-doping of Cu-14 Pc-films with tetrafluorotetracyanoquinodimethane (F4-TCNQ), taking advantage of the good solubility of the Pc (in water and polar solvents) and the strong electron affinity of F4-TCNQ.<sup>85</sup> Remarkably, these films were processed from water solutions (eco-friendly and non-toxic), in a simple manner (mixing of the two components), and at low temperature (reduced cost), thus constituting several advantages for commercialisation purposes. The composite film of Cu-14 with an optimized content of F4-TCNQ dopant (2.5 wt%) showed improved conductivity and hole mobility ( $9.2\times 10^{-3}$   $\text{cm}^2\cdot\text{V}^{-1}\cdot\text{s}^{-1}$ ) by almost two orders of magnitude with respect to that of pristine Cu-14 ( $2.3\times 10^{-4}$   $\text{cm}^2\cdot\text{V}^{-1}\cdot\text{s}^{-1}$ ). Moreover, the pH of the solution of Cu-14 doped with 2.5 wt% of F4-TCNQ is almost neutral (pH = 7.4), in contrast to the acidic character of the standard PEDOT:PSS HTM, which is beneficial for long-term stability of inverted-PSC devices since it limits the corrosion of the electrode. In inverted configuration, the PSCs fabricated with the same optimized composite doped-film (Cu-14+F4-TCNQ-2.5 wt%) showed excellent PCEs of up to 16.14%, which are higher by far than those obtained with the control devices made with pristine Cu-14 (8.7%) or standard PEDOT:PSS (13.22%) HTMs. The modified device retained 88% of the initial value after 350 h of storing in air at room temperature (Fig. 21; with "TS-CuPc" = Cu-14).

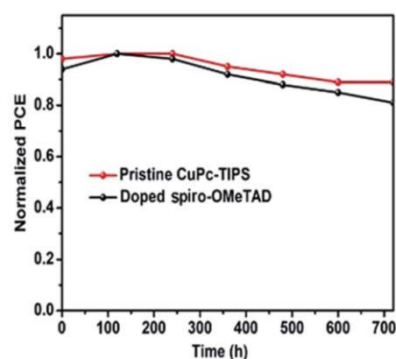


**Fig. 20** PCE variations of PSCs based on pristine CuPc-TIPS and doped spiro-OMeTAD measured under AM1.5 simulated sunlight (100  $\text{mW}\cdot\text{cm}^{-2}$  irradiance); with "CuPc-TIPS" = Cu-6. Reproduced with permission from ref 79 Copyright (2017) Royal Society of Chemistry.

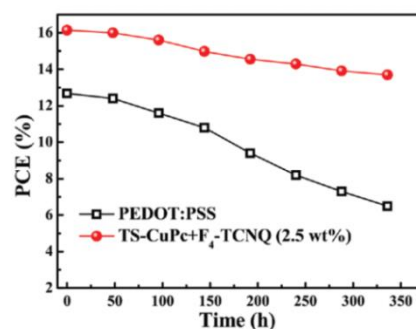


**Fig. 21** PCEs as a function of time in the PEDOT:PSS and TS-CuPc:F4-TCNQ (2.5 wt%) based PSCs without encapsulation under identical storage conditions (in atmosphere, at room temperature); with "TS-CuPc" = Cu-14. Reproduced with permission from ref 85 Copyright (2018) Wiley.

The composite material was also employed as interfacial layer (referred as hole modifying layer) in PSCs within a normal architecture (n-i-p), in which the doped-Pc layer was intercalated between that of *Spiro*-OMeTAD and an Ag counter electrode to form a bi-hole transporting layer. The judiciously aligned energy levels of the three components (perovskite, Cu-14:F4-TCNQ and *Spiro*-OMeTAD) allowed to reduce effectively charge recombination while maintaining a good charge transport within the HTL and without prejudicing hole extraction. Reduced recombination in the modified device was supported by photoluminescence (PL) experiments, the main resulting benefit in the PSCs was, as well as in inverted configuration, an improvement in the FF (0.74), with respect to the devices made with *Spiro*-OMeTAD solely (0.70) or *Spiro*-OMeTAD/undoped-Cu-14 bi-layer (0.70) as HTLs. Accordingly, the *Spiro*/[Cu-14:F4-TCNQ] HTL-bilayered device achieved an excellent maximum PCE of 20.16%, significantly higher than those made with *Spiro*-OMeTAD (16.23%) or *Spiro*/undoped-Cu-14 (16.69%), and presented also reduction in the hysteresis behaviour.

### 2.3. Pcs as dopants or additives

#### 2.3.1. Doping HTMs with Pcs

As an extension of the work discussed above, the same authors reported a later study focused on compositional doping of PEDOT:PSS films with Cu-14 (25 to 60 wt%) to engineer more efficient and stable HTLs for inverted planar PSCs.<sup>86</sup> When Cu-14 was used alone as HTL, poor efficiencies of up to 6.28% were obtained, which was assigned to the poor quality of the Pc films formed over the ITO glass substrate (non-uniformity and large defects). Bilayer configurations, either Pc/PEDOT:PSS or PEDOT:PSS/Pc gave higher PCEs of 10.78% and 13.17%, respectively, but still lower than the 13.29% value of the control device made with PEDOT:PSS solely. At last, improved performances were obtained when using Pc-doped PEDOT:PSS films, with the best values (PCE of 17.29%) obtained for 50 wt% content of Cu-14. The Pc-doped films presented a better uniformity with lower roughness, which is beneficial for the growth of perovskite crystal. This was supported by SEM images, which revealed better crystal quality, lesser defects, and higher coverage of the perovskite when the Pc-doped film was used as under-layer. In addition, these films displayed superior conductivity with respect to the non-doped PEDOT:PSS, which also explained the improved efficiency. Regarding stability matters, the acidic nature of PEDOT:PSS (pH = 2.1 in H<sub>2</sub>O) was only slightly neutralized by the incorporation of the basic Pc (pH = 10.0), since a pH value of 3.3 was obtained for the composite aqueous solution (50 wt% of Pc). Thus, the corrosiveness toward the electrodes was reduced in a lesser extent than in the composite HTL reported in their former work. Nonetheless, more modest but still improved stability was obtained for these cells. Under identical storage conditions and at room temperature, the PCE decreased half of its initial value after 240h for the Pc-doped PEDOT:PSS device and 80h for the control one with PEDOT:PSS only (Fig. 22).

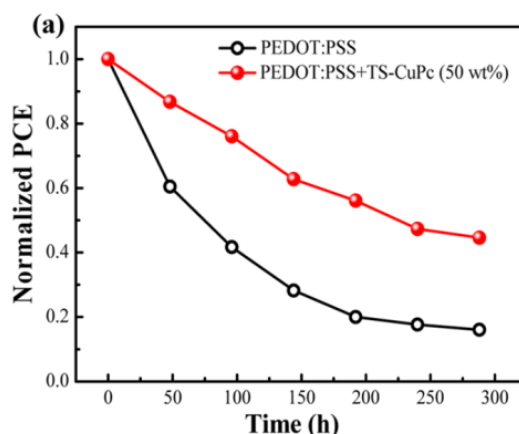


Fig. 22 Normalized PCEs as a function of time in the doped and nondoped PEDOT:PSS-based devices without encapsulation and under identical storage conditions (in atmosphere and at room temperature); with "TS-CuPc" = Cu-15. Reprinted with permission from ref 86 Copyright (2017) American Chemical Society.

An analogous work using Ni-14 as dopant (2.5–15%) for PEDOT:PSS films was reported soon after by the group of Xu, with improved PCE in inverted PSCs of up to 18.90%.<sup>87</sup> Same trends in efficiencies were observed between the single-component and composite HTLs, Ni-14 (9.29%), PEDOT:PSS (16.47%), bi-layered PEDOT:PSS/Pc (13.53%) or Pc/PEDOT:PSS (15.52%), and blended Pc-doped PEDOT:PSS (18.90%). Remarkably, the optimized content of Pc-dopant was much less in this case (10 wt% of Pc) with respect to that reported earlier by Wang et al. with Cu-14 (50 wt%), and higher content of dopant resulted in lower performances (PCE = 16.62% for 15 wt% doping of Pc). Similar conclusions were drawn regarding the effect of the composite HTL, namely, a more effective hole transport, improved morphology of the films, and better stability. In addition, the authors observed enhanced photon absorption in the entire visible range for the Pc-doped PEDOT:PSS films, with respect to those of Ni-14 alone and PEDOT:PSS alone, which, according to the authors, was also a major contribution to such improvement. Three other works have reported on the use of metal Pcs as dopants for HTM in normal *meso*-PSC:  $\beta$ -tetra(n-butyl) (Zn-4)<sup>70</sup> and  $\beta$ -tetra(*tert*-butyl) (Cu-5<sup>71</sup> or Ge-5<sup>62</sup>) Pcs. The study reported by Seo et al. involved Pc-doping (Cu-5)<sup>71</sup> of a molecularly-modified *Spiro*-OMeTAD (*po*-*Spiro*) HTM, in which four over eight *para*-methoxy substituents initially present in the conventional and commercially available *p,p*-*Spiro*-OMeTAD, were changed to the *ortho* position. *po*-*Spiro* HTM doped with an optimized content of Pc (3.8 wt%) and incorporating additives (LiTFSI and TBP), gave the highest performances in PSC with average PCE of 18.2% (max. 20.0%), while the individual components within the same additives composition gave 15.2% for Zn-5 and 17.5% for *po*-*Spiro*. The main contribution came from the FF, with average values of 74.7%, 66.35% and 71.85%, respectively. The authors concluded that a low concentration of Pc-dopant confers to *po*-*Spiro* a more effective capability to block the back flow of electrons from the perovskite layer (*i.e.* reduced recombination), leading to improved FF with respect to the non-doped one. Similarly, Lianos and collaborators found that



doping the standard Spiro-OMeTAD HTM with 10 wt% of *n*-butyl substituted CuPc (Cu-4) increased considerably the efficiency of the PSC up to 15.4% with respect to individual HTMs Cu-4 (8.2%) and Spiro-OMeTAD (10.4%), incorporating LITFSI and TBP additives in the three cases.<sup>70</sup> In agreement with the work of Seo et al. discussed above, same conclusions were drawn regarding the better blocking capability and hence reduced recombination and improved FF within the Cu-4-doped Spiro material. From FE-SEM images, they observed an improvement in the quality of the Spiro-OMeTAD film when doped with the Pc. The authors suggested that Cu-4 may also act as a structural modifier that reduces the size and number of defects, which could constitute an additional explanation for such improvement. Suzuki et al. also obtained improved efficiencies, though much more modest (from 4.23% to 4.47%), when doping Spiro-OMeTAD films with 12.5 wt% of a *tert*-butyl substituted Germanium Pc (Ge-5).<sup>82</sup> However, in contrast to the two previous examples discussed above, they did not obtain improvement in the FF, which was even slightly lower than the non-doped HTM (0.46 vs. 0.51), but in the  $J_{sc}$  (from 10.45 to 15.81 mA/cm<sup>2</sup>). They proposed that Ge-5 dopant promotes carrier generation and diffusion in the Spiro HTL, and help to reduce recombination owing to a better matching of the energy level of the doped-HTM and the perovskite.

### 2.3.2. Pcs as dopants or additives for modified perovskite materials

In a lesser extent, but successfully implemented in PSCs, Pcs have also been considered as dopants or additives for compositional and/or interfacial engineering of the perovskite, targeting to more efficient and stable devices. The infiltration or insertion of these large organic molecules into the perovskite structure can modify its optoelectronic properties and morphology (crystallinity and/or surface coverage), which aims to improve the quality of the film by means of better light-harvesting properties, higher conductivity, lower degree of defects (hence reducing trap-assisted recombination process) or increase interfacial contact with the HTM (hence better charge extraction at the perovskite/HTM interface can be expected). To this end, different approaches have been reported, all of them involving solution-proceeded techniques: (1) direct incorporation into the perovskite precursor solution during the first-step of fabrication of the layer, or (2) during the second one, *via* the mixed-anti solvent technique; (3) by post-treatment (sequential). Concerning the first approach, two independent works were reported by the groups of Behjat,<sup>54</sup> with CuPc in *meso*-type PSC and Peng,<sup>75</sup> with Cu-5 (Cu- $\beta$ -Pc(*tert*butyl)<sub>4</sub>) in a planar configuration. In the first example, an optimal dopant-content of 0.05 wt% Pc in the perovskite material produced significant improvements in performances, with the PCE raising from 6.4% for the non-doped device to 8.4% for the doped one (with Spiro-OMeTAD as the HTL). The main contribution to this enhancement came from an increase in the  $J_{sc}$ , which was attributed to better light-harvesting properties and improvement of quality of the doped-film, specifically, higher degree of crystallinity of the perovskite

structure. Analogously, the second example reports on the doping of the perovskite material with Cu-5 (0.048 wt%) for PSC/Spiro devices in planar configurations, and an improvement in the PCE from 15.3% (without Pc doping) to 17.3% (Pc-doped) was also obtained. Similarly, this improvement was explained by higher quality and crystallinity of the perovskite film with less defective sites, and also higher surface coverage. In a different approach, the groups of Wei and Huang doped the perovskite material (triple-mixed cations) with NiPc using a mixed anti-solvent technique, to obtain improved quality of the film with higher crystallinity.<sup>84</sup> Concretely, after spin-coating the perovskite precursor solution (first step), a solution of NiPc dissolved in the anti-solvent (0.5 mg·mL<sup>-1</sup> in chlorobenzene) was added to the spin-coated substrate in a second step. In this way, the Pc molecules are introduced before completion of the perovskite crystals, and thus can infiltrate into the surface, aiming at increase the interfacial contact between perovskite and hole-transporting layers. In a planar configuration and using Spiro-OMeTAD as HTM, the PCE increased from 17.24% for the non-doped PSC device to 19.18% for the doped one. In the last approach, Cao and co-workers constructed a two-dimensional (2D) modified perovskite 2D-[(ZnPc)<sub>0.5</sub>MA<sub>n-1</sub>PbI<sub>3n+1</sub>] by direct post-treatment of 3D-MAPbI<sub>3</sub> films with a cationic tetra-ammonium ZnPc material (Zn-15).<sup>88</sup> X-ray diffraction (XRD) experiments demonstrated that the Pc molecules were successfully incorporated into the perovskite structure, suturing and thus passivating the grain-boundary (GBs) defects sites initially present in the 3D-lattice of the perovskite. Time-resolved photoluminescence studies indicated a faster decay time for the modified film (57 ns) than the initial one (44 ns), indicating that the passivation of GBs reduced effectively trap-assisted recombination. Consequently, the PSC devices fabricated with the modified 2D Pc-perovskite exhibited fair improvements of all photovoltaic performances ( $V_{oc}$ ,  $J_{sc}$  and F.F.) with a maximum PCE value of 20.3%, higher than the 19.01% value obtained for the best non-modified one. More impacting is the considerably higher stability of the modified device, losing only 10% of its original efficiency after 1000 h when stored at 85 °C and a humidity of ca. 45% (Fig. 23c). In an astonishing comparison, the control device without post-treatment lost over 90% of its original efficiency after only 250 h under the same stressed conditions. As well remarkably, when films of pure and modified perovskite were let to high moisture environment, the colours decayed from dark black to yellow (typically indicative of degradation of perovskite). However, when these films were transferred subsequently to an environment of N<sub>2</sub> at 85°C, only the modified film recovered progressively its initial colour, suggesting a self-repairing capability conferred by the ZnPcs that efficiently suture the GBs of the perovskite.

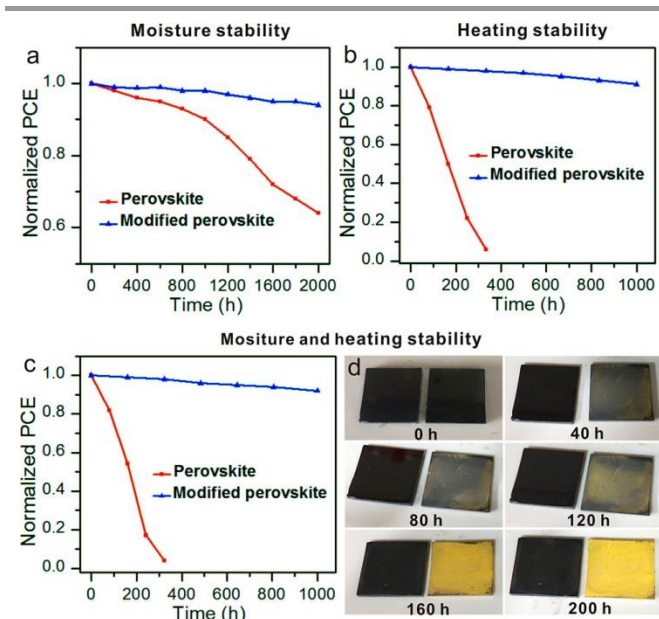


**Fig. 23** (a) Moisture stability measured with a humidity of 45%. (b) Heating stability measured at 85 °C in N<sub>2</sub> environment. (c) Moisture and heating stability tested at 85 °C with a humidity of 45%. (d) The photos of perovskite films with (left) and without (right) modification stored at 85 °C with a humidity of 45% with different time. Reprinted with permission from ref 88 Copyright (2017) American Chemical Society.

## 2.4. Unsymmetrically substituted Pcs

Inducing asymmetry in the Pc scaffold is known to perturb drastically the density and distribution of the 18  $\pi$ -delocalized electrons over the macrocycle, which impact on their photophysical and electrochemical properties, and also the way and strength the Pcs self-aggregate. Given the importance of  $\pi$ - $\pi$  stacking in the morphology and electronic properties of thin film devices discussed above, this kind of Pcs could be interesting to be explored as new materials for HTM. In the field of PSCs, only very few works have considered the use of unsymmetrically substituted Pcs (Fig. 6 and Table 6). The first example was reported by Guo and Zhang with the Pc **CoPcNO<sub>2</sub>-OPh** decorated with three phenoxy and one nitro group at the peripheral  $\beta$ -positions. This Pc displays enough solubility in organic solvent and suitable energy levels to be used as solution-processed HTM in PSC. The dopant-free Pc-based device showed a PCE of 8.24%, fairly close to that obtained with standard doped-Spiro-OMeTAD (10.24%). The same collaborators reported lately three analogues functionalized with three modified (4-methylformate)phenoxy or (4-butyl formate) phenoxy peripheral groups and different metal centres (Cu and Zn), namely **CuPcNO<sub>2</sub>-OMFPh**, **CuPcNO<sub>2</sub>-OBFPPh** and **ZnPcNO<sub>2</sub>-OBFPPh**.

The three Pcs were tested as dopant-free HTMS in double cation (FA/MA) dual-halide (I/Br) mixed PSCs, and achieved improved PCEs of 12.52%, 13.66% and 15.74%, respectively, while the control device made with doped-Spiro-OMeTAD gave 18.42% under these conditions.<sup>99</sup> **ZnPcNO<sub>2</sub>-OBFPPh**-device displayed not only the highest PCE over the three Pcs, but also the least hysteresis behaviour and longest stability, retaining 72.3% of its initial PCE value after 500 h of full sunlight light exposure at 60 °C. In a recent example, Torres and Nazeeruddin introduced a carboxyl group at one  $\beta$ -position of a *tert*-butyl substituted Pc (**TT1**) to induce asymmetry with respect to the symmetrical one with four *tert*-butyl groups (**Zn-5**).<sup>78</sup> The introduction of the carboxyl group, in addition to induce asymmetry of the Pc, may favour the chemical interaction with the perovskite, but no clear evidences could attest if such interaction whether or not exists. The two additive-containing Pc-HTMs were tested in double-cation mixed PSC, and did not show significant differences in terms of efficiency, achieving close and fairly high PCEs of up to 13.7% for **TT1** and 14.0% for **Zn-5** (**TT0** in ref 78).

In a last atypical example, Wang *et al.* reported on the use of two different Pcs integrated in the PSC by dye-sensitization of the mesoporous TiO<sub>2</sub> layer (ETL), acting both as interface modifier layer and co-sensitizer.<sup>100</sup> It is worth to remark that these are the only known examples involving Pcs at the ETL junction of a PSC device. The free-base **Pc-Cou** and zinc **ZnPc-Cou** Pcs both display suitable HOMO-LUMO energy levels to match those of the perovskite (MAPbI<sub>3</sub>) and CB of TiO<sub>2</sub>, which render thermodynamically feasible electron injection from the excited-Pc dyes into the TiO<sub>2</sub>-CB on one hand, and from the perovskite to the Pc-LUMO on the other hand. The devices were fabricated in a conventional *meso*-PSC configuration with MAPbI<sub>3</sub> as perovskite absorber and Spiro-OMeTAD as HTM. The modified Pc-sensitized PSCs showed PCEs of up to 13.55% and 13.96% for **Pc-Cou** and **ZnPc-Cou**, respectively, which are markedly higher in comparison with the control device incorporating solely mesoporous TiO<sub>2</sub> as ETL (10.55%). In particular, higher *J*<sub>SC</sub> values were obtained for the co-sensitized devices, which were assigned to the extra contribution coming from the Pc dyes. This was reflected in their IPCE spectra that showed a greater response in the 400–800 nm region, matching the Pc-absorption features. The higher fill factors were ascribed to lower series resistances, presumably explained by a more favourable morphology of the perovskite layer growth over the Pc-modified layer (fewer grain boundaries). At last, slightly higher *V*<sub>OC</sub> values were obtained and explained by smaller charge recombination resistance as determined from electrochemical impedance spectroscopy (EIS), contributing also, but in a lesser extent, to the improved PCEs.

### 3. Porphyrins and related analogues for perovskite solar cells

Although Pors have played different roles in PSCs, for instance, as additives to enhance the crystallinity of the perovskite layer,<sup>111</sup> as ETL,<sup>112</sup> or as **modifying layer** for interfacial engineering,<sup>113</sup> their potential as HTMs is undeniable if one considers their low oxidation potential and their high hole transporting capabilities, as previously demonstrated in pure organic solar cells.<sup>114–118</sup> As in the case of Pcs, the light-harvesting properties of Pors used as HTM could negatively affect the efficiency of PSCs. However, the number of advantages over Spiro-derivatives and most organic compounds makes them, indeed, candidates of choice. One of the most remarkable features is their high versatility toward structural modification, which opens a path for tuning the photophysical, electrochemical, and charge-transport properties, thus making feasible a sequential improvement of the efficiencies of the PSCs by rational modification of the Por chemical structure. Moreover, Pors offer other valuable features, such as their excellent thermal stability. These advantages have been envisioned by several authors, who have investigated and proved that, as it happens with Pcs, Pors can be successfully incorporated as HTM in PSCs.

Chen, Yeh and co-workers opened a new paradigm of hole-transporters based on Pors with his first report on this topic in 2016.<sup>119</sup> For that purpose, they prepared ZnPors coded as **Y2** and **Y2A2** (Fig. 25, left and Table 7), consisting of a *meso*-5,15-bis(ethynylaniline)porphyrin core, with the nitrogen atom bearing butyl (**Y2**) or dodecyl chains (**Y2A2**), and two facing alkoxyphenyl groups in the other two opposite *meso* positions. The aim of the design is to achieve electronic communication between the Por core and the donor amine groups, and solubility, which is imparted by the lateral alkyl chains. The length of the alkyl chains was shown to have an impact on the film morphology. In fact, **Y2** as thin-film showed both Soret and Q bands red-shifted and significantly broadened with regard to

the thin film of **Y2A2**, indicating stronger intermolecular interaction and, therefore, different surface morphology. On the other hand, these materials present similar HOMO levels at  $-5.25$  and  $-5.10$  eV for **Y2** and **Y2A2**, respectively, comparable with the value of Spiro-OMeTAD at  $-5.22$  eV. PSCs were prepared by spin-coating **Y2** and **Y2A2** solutions (i.e. 70 nm) over the perovskite /mesoporous  $\text{TiO}_2$  layer with 550 nm thickness. The authors observed that **whole** photoluminescence of the perovskite was quenched very efficiently in the presence of either **Y2** or **Y2A2** HTM, which indicated effective hole-extraction by the Por molecules. The  $V_{oc}$  of devices using **Y2** and **Y2A2** were determined as 0.99 and 1.01 V, respectively, only slightly smaller than the  $V_{oc}$  of devices incorporating Spiro-OMeTAD (1.06 V). In addition, the **Y2** device showed  $J_{sc}$  of  $22.82 \text{ mA cm}^{-2}$  and FF of 73.34%, almost identical to Spiro-OMeTAD ( $J_{sc} = 22.79 \text{ mA cm}^{-2}$ ; FF = 74.39%), leading to a PCE of 16.60%, slightly slower than the PCE of Spiro-OMeTAD-based devices (18.03%). **Stability tests over 14 days indicate that Y2-PSC present better moisture resistance stability than Spiro-OMeTAD (Fig. 24).**

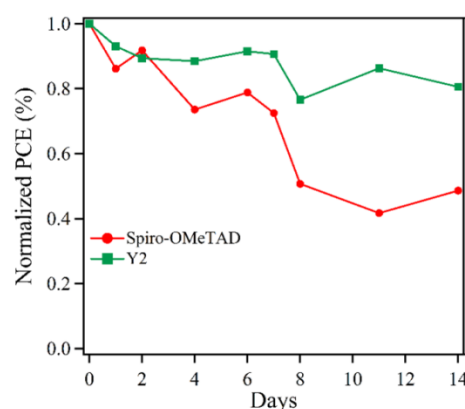


**Fig. 24** Preliminary stability test of perovskite solar cells with different HTMs. Initial PCE values for the devices are 14.84% and 13.81% for Spiro-OMeTAD and **Y2**, respectively. Reproduced from Supporting Information of the article with permission from ref 119. Copyright (2016) American Chemical Society.

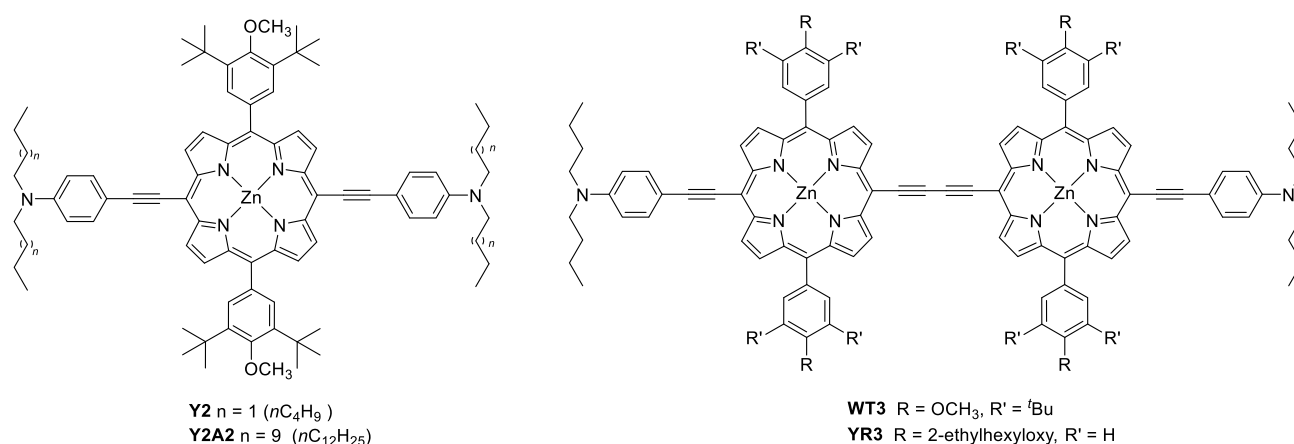


**Fig. 25** Structures of Pors **Y2**, **Y2A2**, **WT3**, and **YR3** in Refs 119 and 120.



Table 7. Work function ( $W_F$ ) of porphyrin-HTMs employed in PSC, and photovoltaic performances of the champion devices under mesoporous (m) or planar (P) configuration.<sup>a</sup>

Por	$W_F$ (eV)	Perovskite composition	Architecture	Type	$J_{sc}$ (mA/cm <sup>2</sup> )	$V_{oc}$ (V)	F.F. (%)	PCE (%)	Ref
Y2	-5.25 <sup>UPS</sup> (-5.22) <sup>EC</sup>	MAPbI <sub>3</sub>	FTO/cTiO <sub>2</sub> /mTiO <sub>2</sub> /perov./Por/Au	m	22.82	0.99	73.34	16.60	119
Y2A2	-5.10 <sup>UPS</sup> (-5.21) <sup>EC</sup>	MAPbI <sub>3</sub>	FTO/cTiO <sub>2</sub> /mTiO <sub>2</sub> /perov./Por/Au	m	17.80	1.01	58.69	10.55	119
WT3	-5.20 <sup>UPS</sup> (-5.14) <sup>EC</sup>	CS <sub>0.05</sub> [(FA <sub>0.83</sub> MA <sub>0.17</sub> )PbI <sub>0.83</sub> Br <sub>0.17</sub> ] <sub>0.95</sub>	FTO/cTiO <sub>2</sub> /mTiO <sub>2</sub> /perov./Por/Au	m	22.60	1.10	78.52	19.44	120
YR3	-5.10 <sup>UPS</sup> (-5.11) <sup>EC</sup>	CS <sub>0.05</sub> [(FA <sub>0.83</sub> MA <sub>0.17</sub> )PbI <sub>0.83</sub> Br <sub>0.17</sub> ] <sub>0.95</sub>	FTO/cTiO <sub>2</sub> /mTiO <sub>2</sub> /perov./Por/Au	m	22.97	1.04	74.75	17.84	120
Y2	-5.22 <sup>UPS</sup> (-5.22) <sup>EC</sup>	CS <sub>0.05</sub> [(FA <sub>0.83</sub> MA <sub>0.17</sub> )PbI <sub>0.83</sub> Br <sub>0.17</sub> ] <sub>0.95</sub>	FTO/cTiO <sub>2</sub> /mTiO <sub>2</sub> /perov./Por/Au	m	22.62	1.09	73.02	17.93	120
Zn-22	-5.29 <sup>EC</sup>	(FAPbI <sub>3</sub> ) <sub>0.85</sub> (MAPbBr <sub>3</sub> ) <sub>0.15</sub>	FTO/cTiO <sub>2</sub> /mTiO <sub>2</sub> /perov./Por/Au	m	22.689	1.099	71.3	17.78	121
Cu-22	-5.37 <sup>EC</sup>	(FAPbI <sub>3</sub> ) <sub>0.85</sub> (MAPbBr <sub>3</sub> ) <sub>0.15</sub>	FTO/cTiO <sub>2</sub> /mTiO <sub>2</sub> /perov./Por/Au	m	21.609	1.072	66.3	15.36	121
PZn-TPA-O	-5.13 <sup>UPS</sup> (-5.08) <sup>EC</sup>	MAPbI <sub>3</sub>	ITO/ZnO/MAPbI <sub>3</sub> /Por/Au	P	19.76	1.031	61.0	12.40	122
PZn-TPA	-5.20 <sup>UPS</sup> (-5.15) <sup>EC</sup>	MAPbI <sub>3</sub>	ITO/ZnO/perov./Por/Au	P	19.35	1.036	60.0	11.96	122
PZn-DPPA-O	-5.23 <sup>UPS</sup> (-5.20) <sup>EC</sup>	MAPbI <sub>3</sub>	ITO/ZnO/perov./Por/Au	P	20.28	1.043	64.0	13.52	122
PZn-DPPA	-5.36 <sup>UPS</sup> (-5.30) <sup>EC</sup>	MAPbI <sub>3</sub>	ITO/ZnO/perov./Por/Au	P	20.74	1.054	65.0	14.11	122
PZn-TPA	-5.20 <sup>UPS</sup> (-5.14) <sup>EC</sup>	MAPbI <sub>3</sub>	ITO/ZnO-s/perov./Por/Au	P	21.07	1.109	70.4	16.37	123
PZn-2FTPA	-5.40 <sup>UPS</sup> (-5.37) <sup>EC</sup>	MAPbI <sub>3</sub>	ITO/ZnO-s/perov./Por/Au	P	22.21	1.125	75.4	18.85	123
PZn-3FTPA	-5.29 <sup>UPS</sup> (-5.24) <sup>EC</sup>	MAPbI <sub>3</sub>	ITO/ZnO-s/perov./Por/Au	P	21.86	1.114	72.7	17.71	123
Zn-Py	-5.35 <sup>th</sup>	MAPbI <sub>3</sub>	FTO/cTiO <sub>2</sub> /mTiO <sub>2</sub> /perov./Por/Au	m	22.29	1.09	73.12	17.82	125
Co(II)-23/Co(III)-23	-5.30/ -5.28 <sup>EC</sup>	CS <sub>x</sub> (MA <sub>0.17</sub> FA <sub>0.83</sub> )(1-x)Pb(I <sub>0.83</sub> Br <sub>0.17</sub> ) <sub>3</sub>	FTO/cTiO <sub>2</sub> /mTiO <sub>2</sub> -SM/perov./Por/Au	m	23.52	1.12	76.01	20.02	126
DPPEZnP-T <sub>2</sub> EH	-5.20 <sup>EC</sup>	MAPbI <sub>3</sub>	ITO/SnO <sub>2</sub> /PCBM/perov./BHJ(Por+PCBM)/MoO <sub>3</sub> /Ag	P	23.32	1.03	78.0	19.02	129

<sup>a</sup>Abbreviations: BHJ = bulk heterojunction; cTiO<sub>2</sub> = compact TiO<sub>2</sub> (blocking layer); FA = formylamidinium; FTO = fluorine doped tin oxide; ITO = indium tin oxide; MA = methylammonium; mTiO<sub>2</sub> = mesoporous TiO<sub>2</sub>; mTiO<sub>2</sub>-SM = mesoporous TiO<sub>2</sub> modified with sinapoyl malate; Por = porphyrin; perov. = perovskite; PCBM = 6,6-phenyl-C<sub>61</sub>-butyric acid methyl ester; ZnO-s = sulfur-passivated ZnO. <sup>b</sup>LITFSI and 4-*tert*-butylpyridine additives were incorporated into the precursor solution for the preparation of the HTL; <sup>c</sup>Work function ( $W_F$ ) of the Por-HTL junction (UPS: determined by ultraviolet photoelectron spectroscopy measurements; EC: value estimated from electrochemical measurements in solutions; th.: value estimated from theoretical calculations).

After this relevant result, the authors prepared two dimeric porphyrin conjugates (**WT3** and **YR3**; Fig. 25, right) related to **Y2**.<sup>120</sup> The design of these molecules with an extended  $\pi$ -conjugation was aimed at increasing the intermolecular interaction in the film and, thus, to achieve enhanced hole mobility. Importantly, these molecules maintained appropriate HOMO levels (-5.14 for **WT3** and -5.11 eV for **Y3**) that ensured minimum energy losses towards charge extraction. With the use of a triple-cation perovskite, the fabricated PSCs using **WT3** and **YR3** showed PCEs of 19.44% and 17.84%, respectively. In particular, Por **WT3** performs better than Spiro-OMeTAD (18.62%), or than the previously reported HTM **Y2** (17.92%) in this type of triple-cation perovskite devices. **WT3**-based device showed excellent moisture, light-soaking and thermal stability, superior to that of Spiro-OMeTAD (Fig. 26). More specifically, it retained more than 90% of the initial PCE after 800 h under a relative humidity of  $\approx$ 40%, whereas that of Spiro-OMeTAD already dropped to 80% after 300 h only under the same conditions. Soon after the first report on Por-based HTMs, the groups of Wong and Zhu described the use of 5,10,15,20-tetrakis{4-[*N,N*-di(4-methoxyphenyl)-aminophenyl]}porphyrin in the form of Zn(II) and Cu(II) complexes (**Zn-22** and **Cu-22**, Fig.

27) as HTLs in PSCs.<sup>121</sup> These symmetrical *meso*-aryl substituted Pors are structurally simpler than **Y2** and **Y2A2**, and can be prepared straightforwardly from low-cost starting materials. An additional advantage is that the bulky and twisted structure of the methoxy-substituted triphenylamine group (as demonstrated by DFT calculations) provides high solubility in common organic solvents. Although these compounds exhibit strong absorption between 400–450 nm, the absorption spectra of TiO<sub>2</sub>/perovskite films with and without **Zn-22** and **Cu-22** layers showed no significant difference for the absorption in the 400–800 nm region, due to the saturated absorption by the perovskite film in this range. The HOMOs of both **Zn-22** (-5.29 eV) and **Cu-22** (-5.37 eV) lie above that of perovskite, with the Cu(II) derivative having a deeper HOMO energy level, which in principle is beneficial for achieving a higher  $V_{oc}$ , but proved unfavourable for hole injection from the perovskite by photoluminescence studies when compared to **Zn-22**-based HTM layers. Eventually, the **Zn-22** PSC provided a PCE of 17.78%, with  $J_{sc}$  of 22.68 mA cm<sup>-2</sup>, a  $V_{oc}$  of 1.099 V, and a FF of 71.3%, whereas **Cu-22** PSCs showed a slightly lower PCE of 15.36%, with the corresponding values of 21.60 mA cm<sup>-2</sup>, 1.072 V, and 66.3%.

## REVIEW ARTICLE

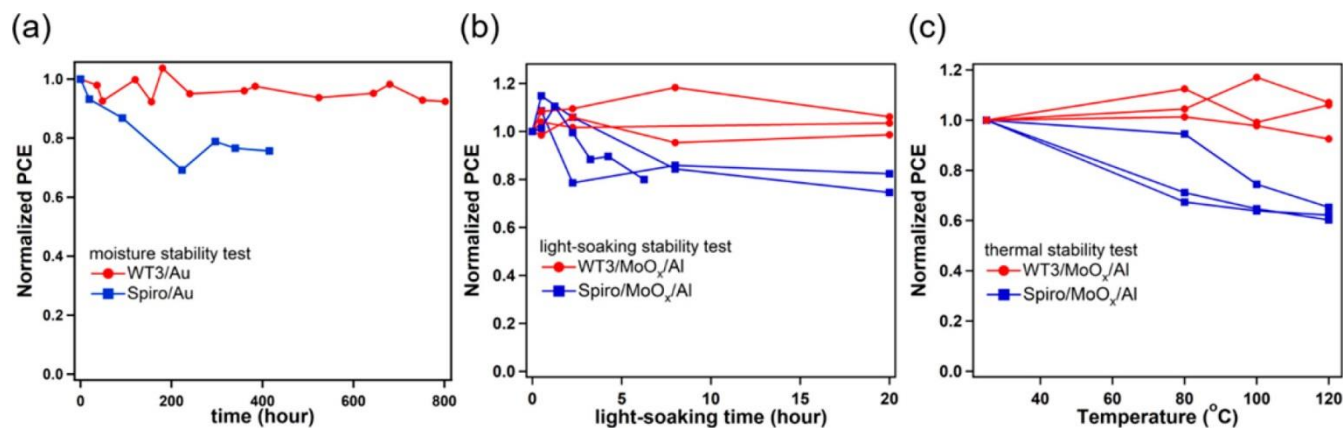


**Fig. 26** Device stability test (without encapsulation) for PSCs with HTMs spiro-OMeTAD or WT3 under different conditions. (a) Moisture stability test for devices stored in a dark environment (RH = 40 ± 10%). (b) Light-soaking stability test (LED, 1 Sun intensity, RH = 15–20%) using MoO<sub>x</sub>/Al as the electrode. (c) Thermal stability test placing MoO<sub>x</sub>/Al-capped devices on the hot plate with varied temperature for 30 min (RH = 15–20%). All J–V curve measurements were conducted at ambient environment (RH = 60 ± 5%) under 1 Sun AM 1.5G illumination. The recorded results are presented with a normalized PCE as a function of storage time or temperature. Reprinted with permission from ref 120. Copyright (2018) American Chemical Society.

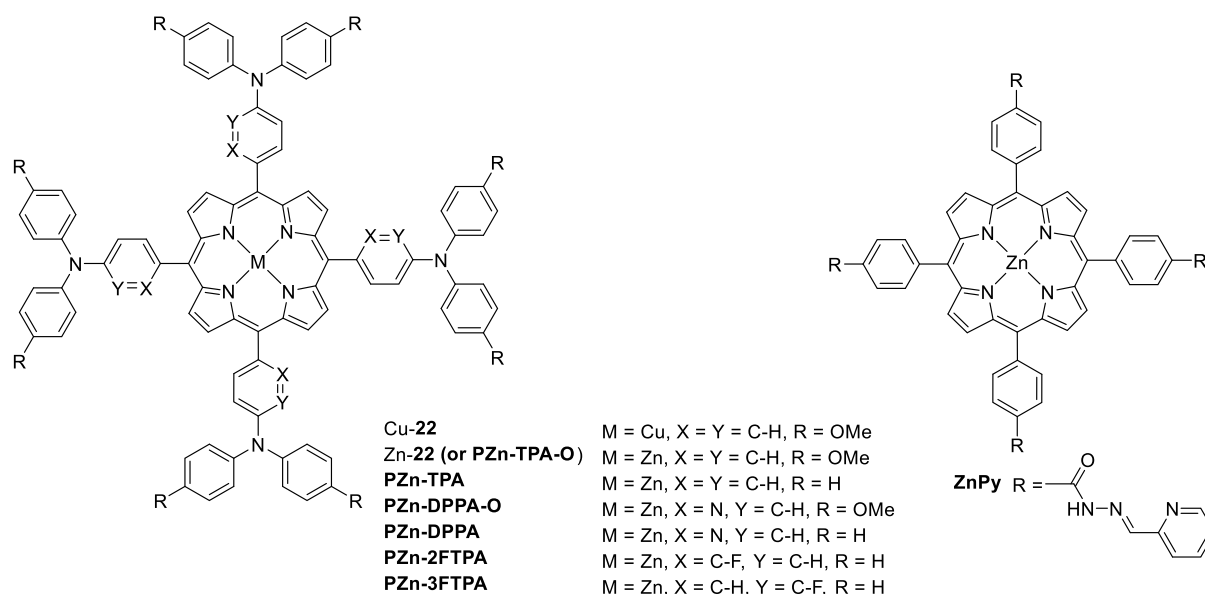


**Fig. 27** Structures of symmetrical tetraaryl-substituted Pors in Refs 121–123 and 125.

Remarkably, Cu-**22** showed a lower  $V_{OC}$  than Zn-**22** in PSCs, in spite of the slightly deeper HOMO level of the former. This was rationalized by the better solubility of Zn-**22** in chlorobenzene, the solvent used for spin-coating the HTM layer, giving rise to a smoother and larger surface coverage than that obtained from Cu-**22** solutions. Importantly, the devices built with Zn-**22** and Cu-**22** rendered similar reproducibility of the PCE than the reference devices constructed with Spiro-OMeTAD (PCE of 18.59%), but much larger stability under ambient conditions (Fig. 28; with "ZnP" = Zn-**22**). Jung and co-workers realized some structural engineering over the previously described symmetrical *meso*-tetraarylamine substituted Pors.<sup>122</sup> These authors synthesized a series of Pors coded as **PZn-TPA-O** (Zn-**22** in reference 121), **PZn-TPA**, **PZn-DPPA-O**, and **PZn-DPPA** (Fig. 27) to investigate the effects of fine-tuning the structure and, therefore, the electronic properties of the Pors, on the device performance. The introduction of an electron-deficient pyridine ring in **PZn-DPPA-O**, and **PZn-DPPA** derivatives realized effective down-shifting of the HOMO energy level, providing a better match to MAPbI<sub>3</sub> perovskite active layer, with regard to pure triphenylamine Pors **PZn-TPA-O** and **PZn-TPA**. On the other hand, the addition of an electron-donating methoxy group in **PZn-TPA-O** and **PZn-DPPA-O** group raised the HOMO energy levels with regard to **PZn-TPA** and **PZn-DPPA** derivatives. Thus, the **PZn-DPPA** showed a HOMO level of  $-5.36$  eV, which is suitable for effective hole extraction and  $V_{OC}$  enhancements in PSC devices. The lowest unoccupied molecular orbital (LUMO) levels of all Pors ( $-3.23$  to  $-3.26$  eV) were sufficiently high compared to those of the perovskite layers ( $-3.90$  eV), confirming the efficient blocking of unwanted electron transfer from MAPbI<sub>3</sub> to HTMs. In this case, the  $V_{OC}$  and the PCEs nearly followed the trend of the HOMO levels, with the **PZn-DPPA**-based devices showing the highest PCE of 14.11%. The superior  $J_{SC}$  value of the **PZn-DPPA** device originated from the improved charge extraction throughout the visible range, as indicated by EQE measurements and transient photovoltage (TPV) spectroscopy. Also, the two DPPA-containing showed greater hole mobility than the TPA-based HTMs, which was attributed to enhanced molecular stacking. **PZn-DPPA** devices, with and without additives, showed superior stability over 25 days under ambient conditions than those made with Spiro-OMeTAD (Fig. 29). Remarkably, although the undoped **PZn-DPPA** device delivered initially a slightly lower PCE than the doped one, its stability was much higher thus retaining the highest PCE after 25 days (92% of its initial value). Further adjusting of the HOMO level of tetra(triphenylamine)-substituted ZnPors was performed by the same authors by introduction of fluorine atoms at 2- or 3- relative positions of the phenyl ring linked to the Por core (**PZn-2FTPA** and **PZn-3FTPA**, Fig. 27 and Table 7).<sup>123</sup> The fluorinated ZnPor-HTMs (**PZn-2FTPA** and **PZn-3FTPA**) exhibited deeper HOMO, enhanced face-on stacking and superior hole transport properties compared to the non-fluorinated derivative **PZn-TPA**. In this work, a device structure was built similarly to the previous work, with the main difference coming from the passivation of the ZnO ETL using 1,2-ethanedithiol. In this case, optimized devices reached PCEs of 16.37% for the

reference **PZn-TPA**, notably higher than the 11.96% value previously reported,<sup>122</sup> and 18.85% and 17.71% for **PZn-2FTPA** and **PZn-3FTPA**, respectively. The doped-**PZn-2FTPA** device retained 90% of its initial PCE after 40 days (relative humidity  $32 \pm 3\%$  without encapsulation), which is improved with respect to the Spiro-OMeTAD one (Fig. 30).

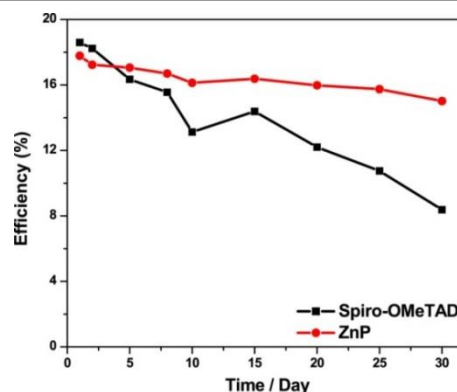


Fig. 28 Stability test of the PSCs employing ZnP and Spiro-OMeTAD without encapsulation, stored under ambient conditions (humidity of about 40–45% and temperature of 20–25 °C; with "ZnP" = Zn-**22**). Reprinted with permission from ref. 121. Copyright (2017) American Chemical Society.

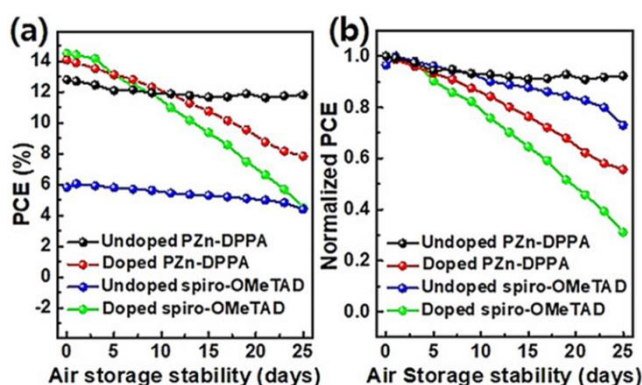


Fig. 29 a) Long-term air stability of PSCs incorporating **PZn-DPPA** and Spiro-OMeTAD with or without dopant; b) normalized PCEs of the corresponding devices. Reproduced with permission from ref 122. Copyright (2017) Wiley.

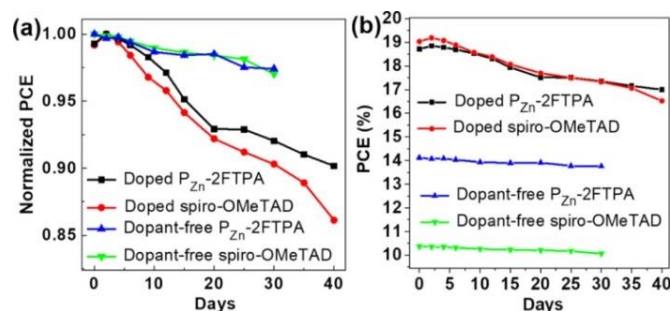


Fig. 30 Air-storage stability of **PZn-2FTPA** and spiro-OMeTAD in the presence and absence of dopants: (a) normalized PCEs and (b) PCEs vs aging time (days). Stability of the devices was measured under the relative humidity of  $32 \pm 3\%$  without encapsulation. Reprinted (adapted) with permission from ref 123. Copyright (2018) American Chemical Society.

Without doping of the HTMs, the stability was enhanced and quite similar both for devices, and although absolute PCE values

were significantly lower than for the doped-ones, that of the Por-device was markedly superior to that of Spiro-OMeTAD within this configuration.

Other authors have performed modifications of the basic *meso*-tetrakis(triphenylamine) substitution in the search of an optimal tuning of the parameters determining the PCE of the device. For instance, Palomares and co-workers have introduced bulky 4-aminophenyl-*N,N*-bis(2',4'-dimethoxy[1,1'-biphenyl]-4-yl) units at the *meso* positions of free base and Zn Por derivatives.<sup>124</sup> These substituents are bulkier and slightly less donating groups than TPA, providing improved solubility and deeper HOMO levels to the ZnPor core (−5.35 and −5.37 eV for the free-base and the Zn complex, respectively). Although mobility measurements have been performed over archetypal ITO/PEDOT:PSS/Por devices, the preparation of PSCs with these materials is still to come. On the other hand, replacement of the TPA moieties by pyridyl-containing phenylacylhydrazone units in the Por core (**ZnPy**) has led to highly efficient (PCE up to 17.8%) PSC devices without p-doping of the HTM layer, showing also much better stability than related Spiro-OMeTAD devices (Fig. 31).<sup>125</sup> The explanation for such features arises from the presence of the pyridine-terminated groups that behave as Lewis bases together with the O and N atoms from acylhydrazone units. These moieties afford efficient electronic passivation of under-coordinated Pb atoms

within the perovskite, as demonstrated by FTIR, and consequently, decreased interfacial charge recombination, as proved by EIS measurements on PSC devices. The TPA-substitution and the ABAB pattern were merged in the Pors used as HTM in PSCs reported by Tang and co-workers.<sup>126</sup> The authors described an original architecture that relies on the use of a natural sunscreen-like molecule (i.e., sinapoyl malate, SM) as interfacial additive to improve both the UV stability of the perovskite and the interfacial contact between TiO<sub>2</sub> and the perovskite layer, and a combination of Co(II) and Co(III) Pors (Co(II)-**23** and Co(III)-**23**, Fig. 32 and Table 7) as HTL.

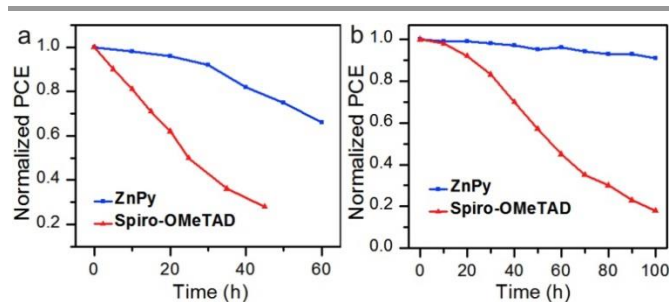


Fig. 31 Stability measured at room temperature with RH of ~70% (a) and at 85 °C in N<sub>2</sub> environment (b) on mesoporous PSCs with Spiro-OMeTAD and ZnPy as HTMs. Reproduced with permission from ref 125. Copyright (2019) Elsevier.

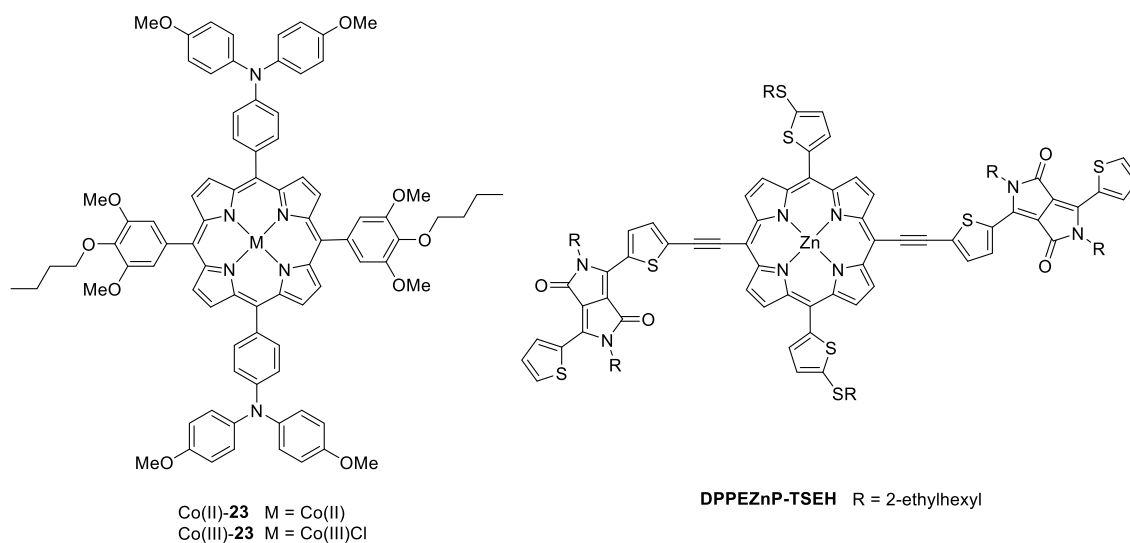
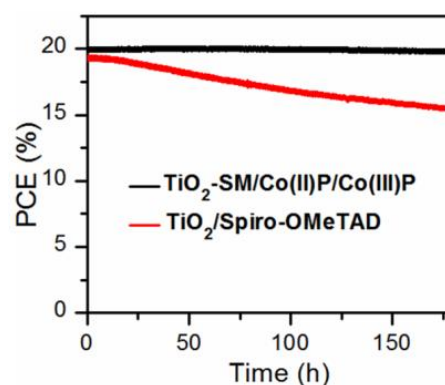


Fig. 32 Structures of ABAB Pors in Refs 126 and 129.

The rationale behind this design is based on the fact that Co(II)/Co(III) is one of the best combinations in oxidation and reduction processes, successfully used as redox couple in DSSCs.<sup>127</sup> The Co-Por molecules were endowed with two facing trialkoxy-substituted phenyl rings to afford solubility, and two opposite methoxy-substituted TPAs that provide efficient hole transport. For the architecture FTO /  $\text{cTiO}_2/\text{mTiO}_2\text{-SM}/\text{Cs}_x(\text{MA}_{0.17}\text{FA}_{0.83})_{1-x}\text{Pb}(\text{I}_{0.83}\text{Br}_{0.17})_3/\text{HTM}/\text{Au}$  (with FA and MA standing for formamidinium and methylammonium cations, respectively) a record efficiency of 20.5% was obtained for a non-doped HTM layer prepared with a mixture Co(II)Por and Co(III)Por in an optimized 4:6 molar ratio. Outstandingly, this value is superior to the 19.6% obtained when using a doped *Spiro*-OMeTAD film as HTL. More importantly, implementation of the Co(II)-**23**/Co(III)-**23** HTL resolved the thermal degradation of PSCs by avoiding ion diffusion of  $\text{I}^-$  and  $\text{MA}^+$  ions from perovskite. As shown in Fig. 33, the PSC device combining  $\text{TiO}_2\text{-SM}$  as ETL and Co(II)-**23**/Co(III)-**23** as HTL, delivers excellent stabilized power output of PCE, with negligible loss over 175 h in comparison with the state-of-the-art device made with *Spiro*-OMeTAD. Other ABAB Pors have been prepared and studied as HTMs,<sup>128</sup> but a remarkable example is that reported by the groups of Peng and Jen, who described a hybrid solar cell comprising a NIR-absorbing bulk heterojunction (BHJ) layer on top of the perovskite, as a way to extend the photoresponse beyond 800 nm and, therefore, enhance the efficiency of perovskite-based solar cells.<sup>129</sup> Hybrid solar cells of this kind incorporate a suitable BHJ mixture working as HTL that has broad light absorption, and suitable energy levels and mobility to simultaneously enhance  $J_{\text{SC}}$ ,  $V_{\text{OC}}$ , and FF with regard to commonly reported PSCs. In this particular case, the BHJ was composed of a NIR-absorbing (band edge at 901 nm) ABAB ZnPor (**DPPEZnP-THE**) and PCBM, which had been previously used as active layer in BHJ devices.<sup>116</sup> The modified version **DPPEZnP-TSEH** (Fig. 32) holds alkyl-sulfide thienyl (instead of alkyl-thienyl) electron-donating groups to adjust the HOMO of the Por (i.e.,  $-5.2$  eV) to match the valence band of perovskite. The S atoms on the side-chains can help also to passivate the trap states of the perovskite crystals. The optimized organic solar cell (OSC) based exclusively on the BHJ of **DPPEZnP-TSEH** and PCBM exhibited a moderate PCE of 7.82% with  $J_{\text{SC}}$ ,  $V_{\text{OC}}$ , and FF up to  $17.35\text{ mA cm}^{-2}$ , 0.79 V, and 0.57, respectively. On the other hand, a reference PSC device with *Spiro*-OMeTAD as HTL exhibits a PCE of 17.56%, with a  $V_{\text{OC}}$  of 1.07 V, a  $J_{\text{SC}}$  of  $21.37\text{ mA cm}^{-2}$ , and a FF of 0.77. Outstandingly, optimized OSC/perovskite hybrid solar cells show a very high PCE of 19.02%, with a  $J_{\text{SC}}$  of  $23.32\text{ mA cm}^{-2}$ , and a FF of 0.78, and a  $V_{\text{OC}}$  of 1.03 V. Transient absorption experiments demonstrated that the BHJ layer contributed to the photocurrent generation not just around the band-edge, but in the entire absorption range of the layer.

All the above mentioned examples refer to changes in the *meso*-substitution of tetraarylPors, which affect the energy levels, absorption properties and intermolecular interactions of the Por core. However, the versatility of Pors and derivatives do not include only variations of the substituents and metal centers, but also structural modifications of the cyclic

tetrapyrrolic ring. Therefore, other tetrapyrrole-based molecules related to porphyrins, such as chlorins (Chl)<sup>130</sup> and bacteriochlorins (BChl),<sup>131</sup> have been also studied as potential HTMs for PSCs. BChls, Chls and Pors possess different degrees of  $\pi$ -conjugation on the ring, which causes differences in their photophysical properties, and thus different hole-extraction abilities. In a recent study,<sup>132</sup> PSCs with a typical mesoporous structure built with three different Zn(II)chlorophyll derivatives having BChl, Chl, and Por macrocycles, showed PCEs of 8.26%, 11.88%, and 0.68%, respectively. This result was rationalized by the most efficient hole extraction capabilities of the BChl ring, as indicated by steady-state photoluminescence, whereas the low PCE (0.68%) of the ZnPor-based PSC was partially ascribed to a small energy gap between its HOMO and the valence band of the perovskite. On the other hand, expanded core-modified porphyrins have been also proposed as materials of choice as HTM for high-performance PSCs.<sup>133</sup>



**Fig. 33** Stabilized power output of PCE at maximum power point as a function of time for the PSCs with  $\text{TiO}_2\text{-SM}$  as ETL and Co(II)P/Co(III)P as HTM (at 0.94 V bias), and the combination of  $\text{TiO}_2$  and *Spiro*-OMeTAD (at 0.91 V bias), measured under AM 1.5G illumination with a relative humidity of 25%. Reproduced from the Supporting Information with permission of ref 126. Copyright (2018) Wiley.

## 4. Conclusions

Phthalocyanines (Pcs) and Porphyrins (Pors) stand out for their low cost of production, high stability and high conductivity in thin films, which render them excellent alternative as economic and efficient hole-transporting materials (HTMs) to be implemented in perovskite solar cells for potential large-scale applications. Over the last four years, excellent efficiencies and, as important, high-stability, have been obtained for PSCs using Pc- and Por-based HTMs, both from vacuum-deposited and solution-processed methods. Several works have demonstrated the crucial importance of  $\pi$ - $\pi$  stacking and aggregated structure of the HTM films toward conductivity, which enhance drastically the efficiency of the PSC device, as well as long-term stability. The high tendency of Pcs and Pors to aggregate into stacks through  $\pi$ - $\pi$  interactions of their macrocycle hence make them ideal candidates for such purpose. Highly ordered columnar stacks with an horizontally alignment (face-to-face) over the perovskite layer can magnify considerably the conductivity of Pc- and Por- films to afford



optimal hole extraction at the interface, which can be achieved by a proper substitution of the macrocycle. In this regard, structural engineering is fundamental for reaching competitive materials that can be an alternative to the benchmark *Spiro-OMeTAD*. Throughout the several reports compiled in this review, it has been indeed demonstrated that both Pcs and Pors are candidates of choice as HTM for the construction of high-performance perovskite solar cells with thermal and moisture stability.

## Conflicts of interest

There are no conflicts to declare.

## Acknowledgements

We are grateful for the financial support of the MINECO, Spain (CTQ2017-85393-P) and the Comunidad de Madrid (FOTOCARBON, S2013/MIT-2841). IMDEA Nanociencia acknowledges support from the 'Severo Ochoa' Programme for Centres of Excellence in R&D (MINECO, Grant SEV-2016-0686). MKN thank the EPFL, and the Swiss National Science Foundation.

## References

- 1 A. Kojima, K. Teshima, Y. Shirai and T. Miyasaka, *J. Am. Chem. Soc.*, 2009, **131**, 6050-6051.
- 2 NREL Best Research-Cell Efficiencies; <https://www.nrel.gov/pv/assets/pdfs/pv-efficiency-chart.20190103.pdf>.
- 3 N. J. Jeon, J. H. Noh, W. S. Yang, Y. C. Kim, S. Ryu, J. Seo and S. I. Seok, *Nature*, 2015, **517**, 476-480.
- 4 J. Burschka, N. Pellet, S.-J. Moon, R. Humphry-Baker, P. Gao, M. K. Nazeeruddin and M. Grätzel, *Nature*, 2013, **499**, 316-319.
- 5 C. Roldán-Carmona, O. Malinkiewicz, A. Soriano, G. Mínguez Espallargas, A. Garcia, P. Reinecke, T. Kroyer, M. I. Dar, M. K. Nazeeruddin and H. J. Bolink, *Energy Environ. Sci.*, 2014, **7**, 994-997.
- 6 S. Wang, Y. Jiang, Emilio J. Juarez-Perez, Luis K. Ono and Y. Qi, *Nat. Energy*, 2016, **2**, 16195.
- 7 B. Conings, J. Drijkoningen, N. Gauquelin, A. Babayigit, J. D'Haen, L. D'Olieslaeger, A. Ethirajan, J. Verbeeck, J. Manca, E. Mosconi, F. D. Angelis and H.-G. Boyen, *Adv. Energy Mater.*, 2015, **5**, 1500477.
- 8 K. T. Cho, G. Grancini, Y. Lee, E. Oveisi, J. Ryu, O. Almora, M. Tschumi, P. A. Schouwink, G. Seo, S. Heo, J. Park, J. Jang, S. Paek, G. Garcia-Belmonte and M. K. Nazeeruddin, *Energy Environ. Sci.*, 2018, **11**, 952-959.
- 9 N. J. Jeon, J. H. Noh, Y. C. Kim, W. S. Yang, S. Ryu and S. I. Seok, *Nat. Mater.*, 2014, **13**, 897.
- 10 M. Jung, S.-G. Ji, G. Kim and S. I. Seok, *Chem. Soc. Rev.*, 2019, DOI: 10.1039/C8CS00656C.
- 11 A. Magomedov, E. Kasparavičius, K. Rakstys, S. Paek, N. Gasilova, K. Genevičius, G. Juška, T. Malinauskas, M. K. Nazeeruddin and V. Getautis, *J. Mat. Chem. C*, 2018, **6**, 8874-8878.
- 12 Z. Ahmad, A. S. Shikoh, S. Paek, M. K. Nazeeruddin, S. A. Al-Muhtaseb, F. Touati, J. Bhadra and N. J. Al-Thani, *J. Mater. Sci.: Mater. Electron.*, 2019, **30**, 1354-1359.
- 13 N. Aristidou, C. Eames, M. S. Islam and S. A. Haque, *J. Mater. Chem. A*, 2017, **5**, 25469-25475.
- 14 G. Kieslich, S. Sun and A. K. Cheetham, *Chem. Sci.*, 2014, **5**, 4712-4715.
- 15 A. D. Jodlowski, C. Roldán-Carmona, G. Grancini, M. Salado, M. Ralaifarisoa, S. Ahmad, N. Koch, L. Camacho, G. de Miguel and M. K. Nazeeruddin, *Nat. Energy*, 2017, **2**, 972-979.
- 16 H. Tsai, W. Nie, J.-C. Blancon, C. C. Stoumpos, R. Asadpour, B. Harutyunyan, A. J. Neukirch, R. Verduzco, J. J. Crochet, S. Tretiak, L. Pedesseau, J. Even, M. A. Alam, G. Gupta, J. Lou, P. M. Ajayan, M. J. Bedzyk, M. G. Kanatzidis and A. D. Mohite, *Nature*, 2016, **536**, 312-316.
- 17 G. Grancini, C. Roldán-Carmona, I. Zimmermann, E. Mosconi, X. Lee, D. Martineau, S. Narbey, F. Oswald, F. De Angelis, M. Grätzel and M. K. Nazeeruddin, *Nat. Commun.*, 2017, **8**, 15684.
- 18 N. Aristidou, C. Eames, I. Sanchez-Molina, X. Bu, J. Kosco, M. S. Islam and S. A. Haque, *Nat. Commun.*, 2017, **8**, 15218.
- 19 Y. Lee, S. Lee, G. Seo, S. Paek, K. T. Cho, A. J. Huckaba, M. Calizzi, D.-w. Choi, J.-S. Park, D. Lee, H. J. Lee, A. M. Asiri and M. K. Nazeeruddin, *Adv. Sci.*, 2018, **5**, 1800130.
- 20 H. Tan, A. Jain, O. Voznyy, X. Lan, F. P. García de Arquer, J. Z. Fan, R. Quintero-Bermudez, M. Yuan, B. Zhang, Y. Zhao, F. Fan, P. Li, L. N. Quan, Y. Zhao, Z.-H. Lu, Z. Yang, S. Hoogland and E. H. Sargent, *Science*, 2017, **355**, 722-726.
- 21 W. Yan, S. Ye, Y. Li, W. Sun, H. Rao, Z. Liu, Z. Bian and C. Huang, *Adv. Energy Mater.*, 2016, **6**, 1600474.
- 22 T. H. Schloemer, J. A. Christians, J. M. Luther and A. Sellinger, *Chem. Sci.*, 2019, **10**, 1904-1935.
- 23 M. Urbani, M. Grätzel, M. K. Nazeeruddin and T. Torres, *Chem. Rev.*, 2014, **114**, 12330-12396.
- 24 L. L. Li and E. W. Diau, *Chem. Soc. Rev.*, 2013, **42**, 291-304.
- 25 M. Urbani, M.-E. Ragoussi, M. K. Nazeeruddin and T. Torres, *Coord. Chem. Rev.*, 2019, **381**, 1-64.
- 26 S. Mathew, A. Yella, P. Gao, R. Humphry-Baker, B. F. Curchod, N. Ashari-Astani, I. Tavernelli, U. Rothlisberger, M. K. Nazeeruddin and M. Grätzel, *Nat. Chem.*, 2014, **6**, 242-247.
- 27 C. G. Claessens, U. Hahn and T. Torres, *Chem. Rec.*, 2008, **8**, 75-97.
- 28 A. W. Snow, 109-Phthalocyanine aggregation in *The Porphyrin Handbook*, eds. K. Kadish, R. Guilard and K. M. Smith, Academic Press, Amsterdam, 2003, vol. 17 pp. 129-176.

- 29 C. F. Van Nostrum and R. J. M. Nolte, *Chem. Commun.*, 1996, 2385-2392.
- 30 M. R. Wasielewski, *Acc. Chem. Res.*, 2009, **42**, 1910-1921.
- 31 J. Elemans, R. van Hameren, R. Nolte and A. Rowan, *Adv. Mater.*, 2006, **18**, 1251-1266.
- 32 H. Imahori, T. Umeyama, K. Kurotobi and Y. Takano, *Chem. Commun.*, 2012, **48**, 4032-4045.
- 33 Y. Miyake, Y. Shiraiwa, K. Okada, H. Monobe, T. Hori, N. Yamasaki, H. Yoshida, M. J. Cook, A. Fujii, M. Ozaki and Y. Shimizu, *Appl. Phys. Express*, 2011, **4**, 021604.
- 34 N. B. Chaure, C. Pal, S. Barard, T. Kreouzis, A. K. Ray, A. N. Cammidge, I. Chambrier, M. J. Cook, C. E. Murphy and M. G. Cain, *J. Mater. Chem.*, 2012, **22**, 19179-19189.
- 35 L. Sosa-Vargas, F. Nekelson, D. Okuda, M. Takahashi, Y. Matsuda, Q.-D. Dao, Y. Hiroyuki, A. Fujii, M. Ozaki and Y. Shimizu, *J. Mat. Chem. C*, 2015, **3**, 1757-1765.
- 36 H. Iino, J.-i. Hanna, R. J. Bushby, B. Movaghar, B. J. Whitaker and M. J. Cook, *Appl. Phys. Lett.*, 2005, **87**, 132102.
- 37 B. C. Nandu, S. Barard, A. K. Ray, A. N. Cammidge and M. J. Cook, *EPL*, 2013, **104**, 57005.
- 38 J. B. Hiroaki Iino and Yukiko Takayashiki and Jun-ichi Hanna and Richard, *Jpn. J. Appl. Phys.*, 2005, **44**, L1310.
- 39 H. Fujikake, T. Murashige, M. Sugibayashi and K. Ohta, *Appl. Phys. Lett.*, 2004, **85**, 3474-3476.
- 40 N. B. Chaure, T. Basova, M. Zahedi, A. K. Ray, A. K. Sharma, M. Durmuş and V. Ahsen, *J. Appl. Phys.*, 2010, **107**, 114503.
- 41 M. Ahmida, R. Larocque, M. S. Ahmed, A. Vacaru, B. Donnio, D. Guillon and S. H. Eichhorn, *J. Mater. Chem.*, 2010, **20**, 1292-1303.
- 42 T. V. Basova, M. Durmuş, A. G. Gürek, V. Ahsen and A. Hassan, *J. Phys. Chem. C*, 2009, **113**, 19251-19257.
- 43 T. Yasuda and T. Tsutsui, *Chem. Phys. Lett.*, 2005, **402**, 395-398.
- 44 C. V. Kumar, G. Sfyri, D. Raptis, E. Stathatos and P. Lianos, *RSC Adv.*, 2015, **5**, 3786-3791.
- 45 N. Torabi, A. Rahnamanic, H. Amrollahi, F. Mirjalili, M. A. Sadeghzade and A. Behjat, *Org. Electron.*, 2017, **48**, 211-216.
- 46 N. Cheng, W. Li, Z. Yu, C. Wang, F. Qi, P. Liu, Y. Xiao and X.-Z. Zhao, *Electrochim. Acta*, 2017, **246**, 990-996.
- 47 F. Zhang, X. Yang, M. Cheng, W. Wang and L. Sun, *Nano Energy*, 2016, **20**, 108-116.
- 48 W. Ke, D. Zhao, C. R. Grice, A. J. Cimaroli, G. Fang and Y. Yan, *J. Mater. Chem. A*, 2015, **3**, 23888-23894.
- 49 Y. Wang, X. Liu, H. Shan, Q. Chen, T. Liu, X. Sun, D. Ma, Z. Zhang, J. Xu and Z.-X. Xu, *Dyes Pigm.*, 2017, **139**, 619-626.
- 50 G. Yang, Y.-L. Wang, J.-J. Xu, H.-W. Lei, C. Chen, H.-Q. Shan, X.-Y. Liu, Z.-X. Xu and G.-J. Fang, *Nano Energy*, 2017, **31**, 322-330.
- 51 Z. Liu, B. Sun, X. Liu, J. Han, H. Ye, Y. Tu, C. Chen, T. Shi, Z. Tang and G. Liao, *J. Mater. Chem. A*, 2018, **6**, 7409-7419.
- 52 J. Han, Y. Tu, Z. Liu, X. Liu, H. Ye, Z. Tang, T. Shi and G. Liao, *Electrochim. Acta*, 2018, **273**, 273-281.
- 53 T. Lei, H. Dong, J. Xi, Y. Niu, J. Xu, F. Yuan, B. Jiao, W. Zhang, X. Hou and Z. Wu, *Chem. Commun.*, 2018, **54**, 6177-6180.
- 54 M. Mozaffari, A. Behjat and N. Torabi, *J. Mater. Sci.: Mater. Electron.*, 2018, **29**, 18187-18192.
- 55 A. Suzuki, T. Kida, T. Takagi and T. Oku, *Jpn. J. Appl. Phys.*, 2016, **55**, 02BF01/01-02BF01/05.
- 56 C. Chen, H. Li, J. Jin, Y. Cheng, D. Liu, H. Song and Q. Dai, *Nano Energy*, 2017, **32**, 165-173.
- 57 C. Chen, H. Li, J. Jin, X. Chen, Y. Cheng, Y. Zheng, D. Liu, L. Xu, H. Song and Q. Dai, *Adv. Energy Mater.*, 2017, **7**, 1700758.
- 58 W. Gao and A. Kahn, *Org. Electron.*, 2002, **3**, 53-63.
- 59 A. Ioakeimidis, C. Christodoulou, M. Lux-Steiner and K. Fostiropoulos, *J. Solid State Chem.*, 2016, **244**, 20-24.
- 60 F. Hou, F. Jin, B. Chu, Z. Su, Y. Gao, H. Zhao, P. Cheng, J. Tang and W. Li, *Sol. Energy Mater. Sol. Cells*, 2016, **157**, 989-995.
- 61 M. Sun, S. Wang, Y. Xiao, Z. Song and X. Li, *J. Energy Chem.*, 2015, **24**, 756-761.
- 62 A. Suzuki, H. Ueda, Y. Okada, Y. Ohishi, Y. Yamasaki and T. Oku, *Chem. Mater. Eng.*, 2017, **5**, 34-42.
- 63 M. Haider, C. Zhen, T. Wu, G. Liu and H.-M. Cheng, *J. Mater. Sci. Technol.*, 2018, **34**, 1474-1480.
- 64 S. Jin, Y. Wei, F. Huang, X. Yang, D. Luo, Y. Fang, Y. Zhao, Q. Guo, Y. Huang and J. Wu, *J. Power Sources*, 2018, **404**, 64-72.
- 65 G. Sfyri, C. V. Kumar, Y.-L. Wang, Z.-X. Xu, C. A. Kroutiras and P. Lianos, *Appl. Surf. Sci.*, 2016, **360**, 767-771.
- 66 X. Liu, Y. Wang, E. Rezaee, Q. Chen, Y. Feng, X. Sun, L. Dong, Q. Hu, C. Li and Z.-X. Xu, *Sol. RRL*, 2018, **2**, 1800050.
- 67 E. Nouri, Y.-L. Wang, Q. Chen, J.-J. Xu, G. Paterakis, V. Dracopoulos, Z.-X. Xu, D. Tasis, M. R. Mohammadi and P. Lianos, *Electrochim. Acta*, 2017, **233**, 36-43.
- 68 E. Nouri, M. R. Mohammadi, Z.-X. Xu, V. Dracopoulos and P. Lianos, *Phys. Chem. Chem. Phys.*, 2018, **20**, 2388-2395.
- 69 G. Sfyri, Q. Chen, Y.-W. Lin, Y.-L. Wang, E. Nouri, Z.-X. Xu and P. Lianos, *Electrochim. Acta*, 2016, **212**, 929-933.
- 70 E. Nouri, Y.-L. Wang, Q. Chen, J.-J. Xu, V. Dracopoulos, L. Sygellou, Z.-X. Xu, M. R. Mohammadi and P. Lianos, *Electrochim. Acta*, 2016, **222**, 1417-1423.
- 71 J. Seo, N. J. Jeon, W. S. Yang, H.-W. Shin, T. K. Ahn, J. Lee, J. H. Noh and S. I. Seok, *Adv. Energy Mater.*, 2015, **5**, 1501320.
- 72 Y. C. Kim, T. Y. Yang, N. J. Jeon, J. Im, S. Jang, T. J. Shin, H. W. Shin, S. Kim, E. Lee, J. H. Noh, S. I. Seok and J. Seo, *Energy Environ. Sci.*, 2017, **10**, 2109-2116.
- 73 T. Duong, J. Peng, D. Walter, J. Xiang, H. Shen, D. Chugh, M. Lockrey, D. Zhong, J. Li, K. Weber, T. P. White and K. R. Catchpole, *ACS Energy Lett.*, 2018, **3**, 2441-2448.
- 74 S. Wu, C. Chen, Q. Liu, T. Peng, R. Li and J. Zhang, *ACS Appl. Energy Mater.*, 2018, **1**, 5539-5547.
- 75 S. Wu, Q. Liu, Y. Zheng, R. Li and T. Peng, *J. Power Sources*, 2017, **359**, 303-310.
- 76 S. Wu, Y. Zheng, Q. Liu, R. Li and T. Peng, *RSC Adv.*, 2016, **6**, 107723-107731.
- 77 K. T. Cho, O. Trukhina, C. Roldán-Carmona, M. Ince, P. Gratia, G. Grancini, P. Gao, T. Marszalek, W. Pisula, P. Y. Reddy, T. Torres and M. K. Nazeeruddin, *Adv. Energy Mater.*, 2017, **7**, 1601733.



- 78 Y. Zhang, S. Paek, M. Urbani, M. Medel, I. Zimmermann, K. T. Cho, M. Ince, M. K. Nazeeruddin and T. Torres, *ACS Appl. Energy Mater.*, 2018, **1**, 2399-2404.
- 79 X. Jiang, Z. Yu, H.-B. Li, Y. Zhao, J. Qu, J. Lai, W. Ma, D. Wang, X. Yang and L. Sun, *J. Mater. Chem. A*, 2017, **5**, 17862-17866.
- 80 P. Qi, F. Zhang, X. Li, Y. Xiao, J. Guo and S. Wang, *Synth. met.*, 2017, **226**, 1-6.
- 81 G. Sfyri, N. Vamshikrishna, C. V. Kumar, L. Giribabu and P. Lianos, *Sol. Energy*, 2016, **140**, 60-65.
- 82 E. Nouri, J. V. S. Krishna, C. V. Kumar, V. Dracopoulos, L. Giribabu, M. R. Mohammadi and P. Lianos, *Electrochim. Acta*, 2016, **222**, 875-880.
- 83 K. T. Cho, K. Rakstys, M. Cavazzini, S. Orlandi, G. Pozzi and M. K. Nazeeruddin, *Nano Energy*, 2016, **30**, 853-857.
- 84 P. Gao, K. T. Cho, A. Abate, G. Grancini, P. Y. Reddy, M. Srivasu, M. Adachi, A. Suzuki, K. Tsuchimoto, M. Grätzel and M. K. Nazeeruddin, *Phys. Chem. Chem. Phys.*, 2016, **18**, 27083-27089.
- 85 J.-M. Wang, Z.-K. Wang, M. Li, C.-C. Zhang, L.-L. Jiang, K.-H. Hu, Q.-Q. Ye and L.-S. Liao, *Adv. Energy Mater.*, 2018, **8**, 1701688.
- 86 J.-M. Wang, Z.-K. Wang, M. Li, K.-H. Hu, Y.-G. Yang, Y. Hu, X.-Y. Gao and L.-S. Liao, *ACS Appl. Mater. Interfaces*, 2017, **9**, 13240-13246.
- 87 X.-F. Zhang, X. Zhou, L. Zhang and B. Xu, *J. Mater. Chem. A*, 2018, **6**, 12515-12522.
- 88 J. Cao, C. Li, X. Lv, X. Feng, R. Meng, Y. Wu and Y. Tang, *J. Am. Chem. Soc.*, 2018, **140**, 11577-11580.
- 89 Y. Wang, X. Zheng, X. Liu, Y. Feng, H. Shan, L. Dong, G. Fang and Z.-X. Xu, *Org. Electron.*, 2018, **56**, 276-283.
- 90 X. Zheng, Y. Wang, J. Hu, G. Yang, Z. Guo, J. Xia, Z. Xu and G. Fang, *J. Mater. Chem. A*, 2017, **5**, 24416-24424.
- 91 F. Javier Ramos, M. Ince, M. Urbani, A. Abate, M. Grätzel, S. Ahmad, T. Torres and M. K. Nazeeruddin, *Dalton Trans.*, 2015, **44**, 10847-10851.
- 92 L. Calio, J. Follana-Berna, S. Kazim, M. Madsen, H.-G. Rubahn, A. Sastre-Santos and S. Ahmad, *Sustainable Energy Fuels*, 2017, **1**, 2071-2077.
- 93 X. Jiang, Z. Yu, J. Lai, Y. Zhang, N. Lei, D. Wang and L. Sun, *Sci. China: Chem.*, 2017, **60**, 423-430.
- 94 X. Jiang, Z. Yu, J. Lai, Y. Zhang, M. Hu, N. Lei, D. Wang, X. Yang and L. Sun, *ChemSusChem*, 2017, **10**, 1838-1845.
- 95 Q.-D. Dao, T. Saito, S. Nakano, H. Fukui, T. Kamikado, A. Fujii, Y. Shimizu and M. Ozaki, *Appl. Phys. Express*, 2013, **6**, 122301.
- 96 Q.-D. Dao, A. Fujii, R. Tsuji, Y. Takeoka and M. Ozaki, *Org. Electron.*, 2017, **43**, 156-161.
- 97 M. Cheng, Y. Li, M. Safdari, C. Chen, P. Liu, L. Kloo and L. Sun, *Adv. Energy Mater.*, 2017, **7**, 1602556.
- 98 J.-J. Guo, X.-F. Meng, J. Niu, Y. Yin, M.-M. Han, X.-H. Ma, G.-S. Song and F. Zhang, *Synth. Met.*, 2016, **220**, 462-468.
- 99 J. Guo, X. Meng, H. Zhu, M. Sun, Y. Wang, W. Wang, M. Xing and F. Zhang, *Org. Electron.*, 2019, **64**, 71-78.
- 100 F. Zhang, S. Wang, Y. Xiao and X. Li, *Synth. Met.*, 2016, **220**, 187-193.
- 101 N. Kobayashi, T. Fukuda, K. Ueno and H. Ogino, *J. Am. Chem. Soc.*, 2001, **123**, 10740-10741.
- 102 T. Fukuda, S. Homma and N. Kobayashi, *Chem. - Eur. J.*, 2005, **11**, 5205-5216.
- 103 M.-E. Ragoussi, J.-J. Cid, J.-H. Yum, G. de la Torre, D. Di Censo, M. Grätzel, M. K. Nazeeruddin and T. Torres, *Angew. Chem., Int. Ed.*, 2012, **51**, 4375-4378.
- 104 M.-E. Ragoussi, J.-H. Yum, A. K. Chandiran, M. Ince, G. de la Torre, M. Grätzel, M. K. Nazeeruddin and T. Torres, *ChemPhysChem*, 2014, **15**, 1033-1036.
- 105 P. Agarwala and D. Kabra, *J. Mater. Chem. A*, 2017, **5**, 1348-1373.
- 106 S. Park, J. H. Heo, J. H. Yun, T. S. Jung, K. Kwak, M. J. Ko, C. H. Cheon, J. Y. Kim, S. H. Im and H. J. Son, *Chem. Sci.*, 2016, **7**, 5517-5522.
- 107 X. Jiang, K. M. Karlsson, E. Gabriellsson, E. M. J. Johansson, M. Quintana, M. Karlsson, L. Sun, G. Boschloo and A. Hagfeldt, *Adv. Funct. Mater.*, 2011, **21**, 2944-2952.
- 108 A. Abate, T. Leijtens, S. Pathak, J. Teuscher, R. Avolio, M. E. Errico, J. Kirkpatrick, J. M. Ball, P. Docampo, I. McPherson and H. J. Snaith, *Phys. Chem. Chem. Phys.*, 2013, **15**, 2572-2579.
- 109 A. Abate, D. J. Hollman, J. Teuscher, S. Pathak, R. Avolio, G. D'Errico, G. Vitiello, S. Fantacci and H. J. Snaith, *J. Am. Chem. Soc.*, 2013, **135**, 13538-13548.
- 110 A. Sadhanala, F. Deschler, T. H. Thomas, S. E. Dutton, K. C. Goedel, F. C. Hanusch, M. L. Lai, U. Steiner, T. Bein, P. Docampo, D. Cahen and R. H. Friend, *J. Phys. Chem. Lett.*, 2014, **5**, 2501-2505.
- 111 T.-H. Chang, C.-W. Kung, H.-W. Chen, T.-Y. Huang, S.-Y. Kao, H.-C. Lu, M.-H. Lee, K. M. Boopathi, C.-W. Chu and K.-C. Ho, *Adv. Mater.*, 2015, **27**, 7229-7235.
- 112 N. Balis, A. Verykios, A. Soultati, V. Constantoudis, M. Papadakis, F. Kournoutas, C. Drivas, M.-C. Skoulikidou, S. Gardelis, M. Fakis, S. Kennou, A. G. Kontos, A. G. Coutsolelos, P. Falaras and M. Vasilopoulou, *ACS Appl. Energy Mater.*, 2018, **1**, 3216-3229.
- 113 B. Li, C. Zheng, H. Liu, J. Zhu, H. Zhang, D. Gao and W. Huang, *ACS Appl. Mater. Interfaces*, 2016, **8**, 27438-27443.
- 114 M. V. Martínez-Díaz, G. de la Torre and T. Torres, *Chem. Commun.*, 2010, **46**, 7090-7108.
- 115 H. Qin, L. Li, F. Guo, S. Su, J. Peng, Y. Cao and X. Peng, *Energy Environ. Sci.*, 2014, **7**, 1397-1401.
- 116 K. Gao, L. Li, T. Lai, L. Xiao, Y. Huang, F. Huang, J. Peng, Y. Cao, F. Liu, T. P. Russell, R. A. J. Janssen and X. Peng, *J. Am. Chem. Soc.*, 2015, **137**, 7282-7285.
- 117 S. Chen, L. Xiao, X. Zhu, X. Peng, W.-K. Wong and W.-Y. Wong, *Chem. Commun.*, 2015, **51**, 4439-4442.
- 118 H. Wang, L. Xiao, L. Yan, S. Chen, X. Zhu, X. Peng, W.-K. Wong and W.-Y. Wong, *Chem. Sci.*, 2016, **7**, 4301-4307.
- 119 H.-H. Chou, Yu.-H. Chiang, M.-H. Li, P.-S. Shen, H.-J. Wei, C.-L. Mai, P. Chen and C.-Y. Yeh, *ACS Energy Lett.*, 2016, **1**, 956-962.

- 120 Y.-H. Chiang, H.-H. Chou, W.-T. Cheng, Y.-R. Li, C.-Y. Yeh and P. Chen, *ACS Energy Lett.*, 2018, **3**, 1620-1626.
- 121 S. Chen, P. Liu, Y. Hua, Y. Li, L. Kloo, X. Wang, B. Ong, W.-K. Wong and X. Zhu, *ACS Appl. Mater. Interfaces*, 2017, **9**, 13231-13239.
- 122 U.-H. Lee, R. Azmi, S. Sinaga, S. Hwang, S. H. Eom, T.-W. Kim, S. C. Yoon, S.-Y. Jang and I. H. Jung, *ChemSusChem*, 2017, **10**, 3780-3787.
- 123 R. Azmi, U.-H. Lee, F. T. H. Wibowo, S. H. Eom, S. C. Yoon, S.-Y. Jang and I. H. Jung, *ACS Appl. Mater. Interfaces*, 2018, **10**, 35404-35410.
- 124 R. Pudi, C. Rodríguez-Seco, A. Vidal-Ferran, P. Ballester and E. Palomares, *Eur. J. Org. Chem.*, 2018, **2018**, 2064-2070.
- 125 X. Lva, G. Xiaoa, X. Fengb, J. Caob, X. Yaoa, J. Liua, *Dyes Pigm.*, 2019, **160**, 957-961.
- 126 J. Cao, X. Lv, P. Zhang, T. T. Chuong, B. Wu, X. Feng, C. Shan, J. Liu and Y. Tang, *Adv. Mater.*, 2018, **30**, 1800568.
- 127 A. Yella, H.-W. Lee, H. N. Tsao, C. Yi, A. K. Chandiran, M. K. Nazeeruddin, E. W.-G. Diau, C.-Y. Yeh, S. M. Zakeeruddin and M. Grätzel, *Science*, 2011, **334**, 629-634.
- 128 D. Sygkridou, A. Apostolopoulou, A. Charisiadis, V. Nikolaou, G. Charalambidis, A. G. Coutsolelos and E. Stathatos, *ChemistrySelect*, 2018, **3**, 2536-2541.
- 129 K. Gao, Z. Zhu, B. Xu, S. B. Jo, Y. Kan, X. Peng and A. K.-Y. Jen, *Adv. Mater.*, 2017, **29**, 1703980.
- 130 M. Li, Y. Li, S. Sasaki, J. Song, C. Wang, H. Tamiaki, W. Tian, G. Chen, T. Miyasaka and X.-F. Wang, *ChemSusChem*, 2016, **9**, 2862-2869.
- 131 M. Li, S. Sasaki, Y. Sanehira, T. Miyasaka, H. Tamiaki, T. Ikeuchi, G. Chen and X.-F. Wang, *J. Photochem. Photobiol. A*, 2018, **353**, 639-644.
- 132 M. Li, N. Li, W. Hu, G. Chen, S. Sasaki, K. Sakai, T. Ikeuchi, T. Miyasaka, H. Tamiaki, X.-F. Wang, *ACS Appl. Energy Mater.* 2018, **1**, 9-16.
- 133 S. B. Mane, A. A. Sutanto, C.-F. Cheng, M.-Y. Xie, C.-I. Chen, M. Leonardus, S.-C. Yeh, B. B. Beyene, E. W.-G. Diau, C.-T. Chen and C.-H. Hung, *ACS Appl. Mater. Interfaces* 2017, **9**, 31950-31958.